



## LJMU Research Online

**Bie, C, Ma, Y, van Zijl, PCM, Yadav, NN, Xu, X, Zheng, H, Liang, D, Zou, C, Areta, JL, Chen, L and Zhou, Y**

**In vivo imaging of glycogen in human muscle**

<http://researchonline.ljmu.ac.uk/id/eprint/25122/>

### Article

**Citation** (please note it is advisable to refer to the publisher's version if you intend to cite from this work)

**Bie, C, Ma, Y, van Zijl, PCM, Yadav, NN, Xu, X, Zheng, H, Liang, D, Zou, C, Areta, JL, Chen, L and Zhou, Y (2024) In vivo imaging of glycogen in human muscle. Nature Communications, 15. pp. 1-14. ISSN 2041-1723**

LJMU has developed **LJMU Research Online** for users to access the research output of the University more effectively. Copyright © and Moral Rights for the papers on this site are retained by the individual authors and/or other copyright owners. Users may download and/or print one copy of any article(s) in LJMU Research Online to facilitate their private study or for non-commercial research. You may not engage in further distribution of the material or use it for any profit-making activities or any commercial gain.

The version presented here may differ from the published version or from the version of the record. Please see the repository URL above for details on accessing the published version and note that access may require a subscription.

For more information please contact [researchonline@ljmu.ac.uk](mailto:researchonline@ljmu.ac.uk)


<http://researchonline.ljmu.ac.uk/>

# In vivo imaging of glycogen in human muscle

Received: 26 February 2024

Accepted: 3 December 2024

Published online: 30 December 2024

 Check for updatesChongxue Bie<sup>1</sup>, Yuxuan Ma<sup>1</sup>, Peter C. M. van Zijl<sup>2,3</sup>, Nirbhay N. Yadav<sup>2,3</sup>, Xi Xu<sup>1</sup>, Hairong Zheng<sup>1</sup>, Dong Liang<sup>1</sup>, Chao Zou<sup>1</sup>, José L. Areta<sup>4</sup>, Lin Chen<sup>5</sup> & Yang Zhou<sup>1</sup>✉

Probing regional glycogen metabolism in humans non-invasively has been challenging due to a lack of sensitive approaches. Here we studied human muscle glycogen dynamics post-exercise with a spatial resolution of millimeters and temporal resolution of minutes, using relayed nuclear Overhauser effect (glycoNOE) MRI. Data at 5T showed a homogeneous distribution of glycogen in resting muscle, with an average concentration of  $99 \pm 13$  mM. After plantar flexion exercise following fasting with recovery under fasting conditions, the calf muscle showed spatially heterogeneous glycogen depletion and repletion kinetics that correlated with the severity of this depletion. Three types of regional glycogen kinetics were observed: (i) single exponential repletion (type a); (ii) biphasic recovery of rapid repletion followed by additional depletion (type b); (iii) biphasic recovery where continued depletion is followed by an exponential recovery (type c). The study of the complex patterns of glycogen kinetics suggests that glycogen breakdown may be quantitatively important during the initial recovery.

In humans, the majority of D-glucose taken up is deposited as muscle glycogen<sup>1,2</sup> (~400 g in total) with a resting concentration of around 100 mM (glucose units) in healthy controls<sup>3,4</sup>. During exercise, muscle glycogen is consumed to maintain a continuous supply of adenosine triphosphate, with glycogen metabolic rates depending on the exercise intensity of a particular muscle and its duration<sup>5</sup>. When performing a contractile task (e.g., plantar flexion), muscles are recruited with intensities that vary within the same muscle and among different muscle groups<sup>6–9</sup>. This may lead to spatially heterogeneous muscular glycogen utilization and storage at both macroscopic (muscle group)<sup>10,11</sup> and subcellular levels<sup>12,13</sup>. At recovery, the exercised muscles resynthesize glycogen mainly from blood D-glucose via a multiple-step enzymatic regulation (e.g., D-glucose transporter, hexokinase, and glycogen synthase (GSase))<sup>14</sup>, a process that is also regulated locally<sup>15</sup>. In the context of this metabolic heterogeneity and complex regulation, the spatial characterization of glycogen usage and recovery in situ would deepen our understanding of muscle metabolic regulation and disorders.

The quantification of human glycogen in situ has relied mainly on the use of <sup>13</sup>C magnetic resonance spectroscopy (MRS), pioneered by

Shulman and colleagues<sup>3,15–17</sup> in the 1980s and 1990s. These in vivo <sup>13</sup>C MRS studies on glycogen depletion<sup>17</sup>, turnover<sup>18</sup>, and re-synthesis<sup>3,19</sup> in humans have greatly facilitated the quantitative understanding of glycogen metabolic regulation. In a series of <sup>13</sup>C studies on human muscle glycogen<sup>3,20</sup>, it was shown that glycogen synthesis in skeletal muscle after intensive exercise is biphasic with a rapid repletion phase followed by a slower one. Based on the in vivo <sup>13</sup>C MRS data, it was proposed that either D-glucose transport or its phosphorylation with hexokinase is the rate-controlling factor for glycogen re-synthesis<sup>21</sup>, challenging a previously generally accepted model of GSase controlling glycogen re-synthesis in muscle. However, due to the low detection sensitivity of <sup>13</sup>C MRS, the measurements of total glycogen at natural abundance (1.1%) are often performed in a large volume with a low temporal resolution<sup>16</sup>. As a result, it is difficult for <sup>13</sup>C MRS to assess the inherent spatial heterogeneity of glycogen metabolism in tissues<sup>15,22</sup>. Furthermore, <sup>13</sup>C MRS requires additional hardware that is not widely available on human scanners, and only a limited number of in vivo studies have been reported so far. Over the years, the idea has also advanced that muscle glycogen re-synthesis after exercise occurs not solely through mechanisms via D-glucose

<sup>1</sup>Shenzhen Institute of Advanced Technology, Chinese Academy of Sciences, Shenzhen, Guangdong, China. <sup>2</sup>F.M. Kirby Research Center for Functional Brain Imaging, Kennedy Krieger Institute, Baltimore, MD, USA. <sup>3</sup>The Russell H. Morgan Department of Radiology, The Johns Hopkins University School of Medicine, Baltimore, MD, USA. <sup>4</sup>Research Institute for Sport and Exercise Sciences, School of Sport and Exercise Sciences, Liverpool John Moores University, Liverpool, UK. <sup>5</sup>School of Electronic Science and Engineering, Xiamen University, Xiamen, Fujian, China. ✉e-mail: [yang.zhou@siat.ac.cn](mailto:yang.zhou@siat.ac.cn)

uptake and GSase, but also glycogen phosphorylase (GPase)<sup>23–25</sup>. It was shown recently that the inactivation of GPase accounted for 45–75% of glycogen accumulation in isolated muscle during the initial recovery from repeated contractions<sup>26–28</sup>. The inhibition of GPase has thus been suggested to play an active role during glycogen re-synthesis<sup>27</sup>. To date, whether glycogen breakdown is quantitatively important during muscle recovery *in vivo* remains controversial.

Saturation transfer (ST) MRI is an approach in which nuclear pools (generally protons) in molecules are saturated and the saturation is transferred to other molecules<sup>29</sup>. Recent types of ST MRI allow imaging of molecular information through the water signal with a large sensitivity enhancement. This includes molecules with protons exchanging with water (e.g., –NH, –NH<sub>2</sub>, –OH), in a process called chemical exchange saturation transfer (CEST)<sup>30,31</sup>, as well as molecules that are magnetically coupled with water via the relayed nuclear Overhauser effects (rNOE)<sup>30,32</sup>. The latter has been named relayed nuclear Overhauser enhancement (rNOE)<sup>30,32</sup> for mobile macromolecules and conventional magnetization transfer contrast (MTC) for solid-like molecules<sup>33–36</sup>. For instance, CEST MRI has recently gained increasing popularity in (pre)clinical studies as a molecular imaging approach for several energy metabolites (e.g., creatine<sup>37,38</sup> and phosphocreatine (PCr)<sup>39,40</sup>). In CEST and rNOE-based MRI, analogous to a <sup>1</sup>H MR spectrum, a water saturation spectrum or Z-spectrum can be acquired to show the resonances of proton pools of different molecular origins. Previous studies on animal liver have shown that the rNOE between glycogen and water (glycoNOE) in ST experiments<sup>41</sup> can be used to enhance glycogen aliphatic proton signals by two orders of magnitude relative to proton MRS, thus suggesting a path toward mapping glycogen kinetics with MRI at high tempo-spatial resolution *in vivo*<sup>42</sup>.

Here, we used glycoNOE MRI to study the regional kinetics of exercise-induced muscle glycogen depletion and repletion in humans. We first established the glycoNOE approach to map glycogen in human calf muscle at rest. The spatial distribution of glycogen in muscle was determined by calibrating the *in vivo* glycoNOE signal to a known concentration relationship from *in vitro* glycogen samples with granule sizes similar to those in human muscle. We then monitored glycogen depletion and repletion over up to 6 h after a plantar flexion exercise protocol in volunteers with lower and higher intensity exercise. We found three types of glycogen repletion kinetics in the local regions of exercised muscles. The successful imaging of glycogen kinetics allows the analysis of complex patterns of glycogen depletion and recovery in humans at high resolution.

## Results

### The measurement of glycogen in resting human muscle

We first aimed to establish the approach to measure glycogen in human muscle *in situ* with MRI at 5T. Figure 1a shows a Z-spectrum for glycogen (with an average size of 26 nm, see size distribution in Supplementary Fig. 1) in solution *in vitro* (pH 7.3, 37 °C) at 5T. The glycoNOE(26 nm) signals around –1 ppm were quantified as the peak integral of the difference signal after fitting the Lorentzian-shaped water direct saturation (DS) background and subtracting it out. The glycoNOE (26 nm) signals in solution were linearly correlated with the glycogen concentrations ([Gly], in glucose units) over the concentration range studied (Fig. 1b). To mimic and investigate the effects of tissue MTC background on glycoNOE signals in the Z-spectrum *in vivo*, glycogen was also prepared and measured in solidified 1% agar (see its MTC background in Supplementary Fig. 2) *in vitro*. The slopes of the signal-concentration curves for samples in solution and in 1% agar were comparable for B<sub>1</sub> = 0.2 μT (Fig. 1b), giving the following calibration equation:

$$[\text{Gly}] = \text{glycoNOE (26 nm)} / \text{slope (26 nm)} \quad (1)$$

where slope(26 nm) = 0.115 ± 0.003 signal units/mM for glycogen at 26 nm. Figure 1c shows that the measured glycoNOE increases with

glycogen particle size (*d*) in the range of 12 nm to 28 nm *in vitro* (100 mM, pH 7.3), and that the dependence of relative glycoNOE signals on particle size (*d*) can be described by:

$$\alpha(d) = \text{glycoNOE}(d) / \text{glycoNOE}(26 \text{ nm}) = 0.0004 \times d^2 + 0.0287 \times d - 0.0176 \quad (2)$$

where glycoNOE(*d*) denotes the glycoNOE signal at particle size *d*, α(*d*) is defined as the size factor (α(26 nm) = 1), and its expression was obtained by fitting the curve in Fig. 1c with a binomial equation. Figure 1d shows a representative Z-spectrum of the calf muscle for one of the 16 volunteers studied at rest. A difference spectrum is constructed by subtracting the Z-spectrum from the estimated background of MTC and DS (see Supplementary Methods and Supplementary Fig. 3), after which the glycoNOE peak becomes visible at –1 ppm (Fig. 1d). The signals are affected by B<sub>1</sub> and the optimal B<sub>1</sub> in skeletal muscle was determined to be 0.2 μT for glycoNOE signals (Fig. 1e). Signal biases due to the spatial B<sub>0</sub> and B<sub>1</sub> inhomogeneity (Fig. 1g, h) were corrected voxel-by-voxel (see B<sub>1</sub> correction in Supplementary Fig. 4). By using a two-step multi-pool Lorentzian fitting, the glycoNOE peak at –1 ppm was quantified. After voxel-by-voxel fitting and using the *in vitro* calibrations at 26 nm (Fig. 1b), a glycogen concentration map for skeletal muscle was obtained (Fig. 1i), showing an approximately homogeneous distribution of the glycogen in rested muscle. The glycoNOE signal integral in calf muscle for 16 subjects was 11.4 ± 1.5% ppm (Fig. 1e) on average, corresponding to 99 ± 13 mM glycogen. Repetitive scans conducted for each subject found that the standard deviation (SD) of measured glycogen in muscle decreased with increasing volume size and was about 13 mM for 1 cm<sup>3</sup> muscle tissue.

### Mapping muscle glycogen dynamics under exercise

We then studied the dynamics of exercise-induced glycogen depletion and post exercise repletion in human skeletal muscle with MRI. The calf muscle of 14 healthy volunteers was monitored before and up to 6 h after a protocol of 31 min of plantar flexion exercise<sup>3</sup> (Fig. 2 and Supplementary Fig. 5), in which volunteers were asked to alternate 1 min of single-leg calf raises and 1 min of rest with an estimated total mechanical work of 11 to 23 kJ. Their blood glucose levels were 5.1 ± 0.2 mM, 4.9 ± 0.3 mM, and 4.8 ± 0.4 mM before exercise, 3 h, and 6 h after exercise, respectively. Considering that glycogen particle size was correlated with glycogen concentration in exercised muscle in humans (Supplementary Table 1 and Supplementary Fig. 6), we estimated the glycogen concentration maps from glycoNOE signals for muscles at each time point post exercise based on the *in vitro* dependence (Fig. 1b, c) of glycoNOE on the glycogen particle size and concentration (see Methods). Immediately after exercise, the extracted glycoNOE signals for a representative subject (Fig. 2a–c) showed substantial glycogen depletion from 108 mM pre-exercise to 52 mM at 13 min post exercise and 76 mM at 6 h post exercise. The glycogen maps obtained post exercise showed a heterogeneous distribution of glycogen within the calf muscle (Fig. 2d, muscle groups assigned based on T<sub>2w</sub> MRI). The muscle glycogen in different regions started to recover over the 6 h post exercise, but never reached its original levels (Fig. 2d), which is expected when no additional carbohydrate supplements are provided<sup>43</sup>. The muscle groups of this representative subject showed exponential recovery with different rates, with the medial gastrocnemius (MG) regions showing the most rapid recovery (Fig. 2e and Supplementary Fig. 7). The muscle glycogen repletion kinetic data were fitted voxel-by-voxel with a single exponential model, giving the estimated glycogen concentrations at any time points post exercise, including at *t* = 0 ([Gly(0)]) and steady state ([Gly]<sup>ss</sup>). By comparing glycogen at the base level ([Gly]<sup>base</sup>) pre-exercise with estimated [Gly(0)] post exercise, Fig. 2f shows a map of the amount of glycogen depleted by the exercise (Δ[Gly(0)]<sub>dep</sub><sup>ex</sup> = [Gly]<sup>base</sup> – [Gly(0)]).

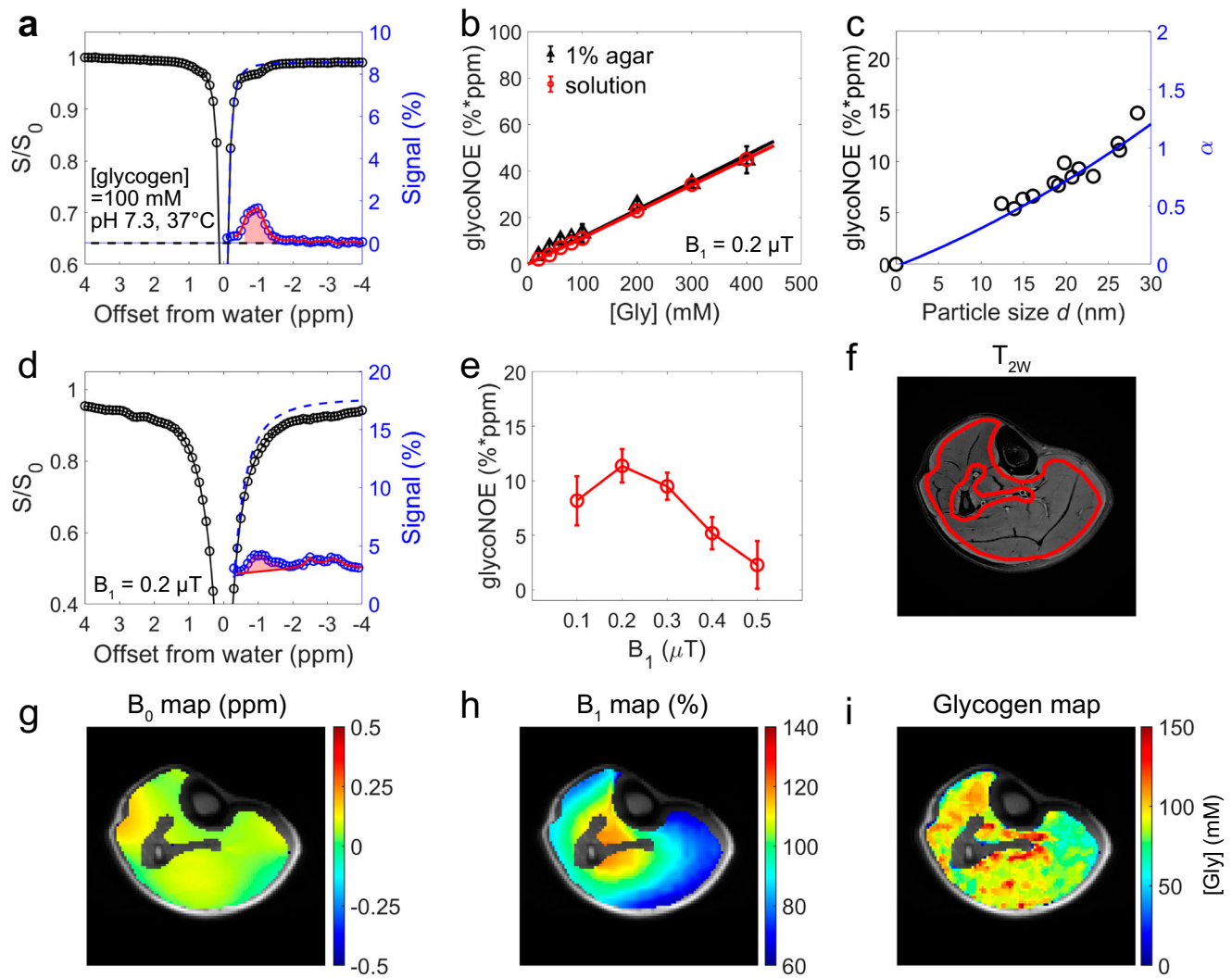


**Fig. 1 | Measurement of muscle glycogen at 5T. a, b** Spectral quantification and concentration calibration of glycoNOE from Z-spectra of glycogen at 26 nm in vitro (pH 7.3, 37°C) both in neat solution and in agar to simulate tissue. The average and standard values of glycoNOE(26 nm) signals were obtained from two separate acquisitions ( $n = 2$  acquisitions). **c** The relative glycoNOE signal ( $\alpha$ ) as a function of particle size. The signals were normalized using glycoNOE at 26 nm. The curve was fitted using Eq. 2. **d** Extraction of in vivo glycoNOE signal from the red area under the curve of the difference signal between Z-spectrum (black

circles) with Lorentzian water line fit (blue dashes). **e** The glycoNOE signal in vivo as a function of  $B_1$  ( $n = 16$  subjects), showing a reduction above  $0.2 \mu\text{T}$  due to background interference. **f** Outline of region of interest in human skeletal muscle used for the spectra. **g, h** The  $B_0$  and  $B_1$  maps. **i** Glycogen concentration map over a slice through the calf, based on glycoNOE after  $B_0$  and  $B_1$  correction and calibrated using (b). Slice thickness = 5 mm,  $B_1 = 0.2 \mu\text{T}$ ,  $t_{\text{sat}} = 3$  s,  $\text{TR} = 4$  s. Data in (b) and (e) are presented as means  $\pm$  SD. Source data are provided as a Source Data file.

Figure 2g, h shows maps of glycogen repletion amount over the first 3 h ( $\Delta[\text{Gly}(3\text{h})]_{\text{rep}} = [\text{Gly}(3\text{h})] - [\text{Gly}(0)]$ ) and initial repletion rates (initial slope of exponential recovery,  $R_{\text{rep}}^{\text{initial}}$ , in units of mM/h, Supplementary Fig. 7), indicating a heterogeneous distribution of glycogen repletion processes over the calf slice. The initial repletion rate  $R_{\text{rep}}^{\text{initial}}$  reached as high as about 140 mM/h in the core region of the MG muscle for this representative subject (Fig. 2g), which correlated well spatially with the region where glycogen was heavily depleted (Fig. 2f). While several individual subjects showed clear exponential recovery within the muscle regions as assigned based on  $T_{2w}$  MRI, when assessing the data of 14 participants (Fig. 2i–k), the average curves could not be distinguished within error from a slow linear repletion of glycogen levels. The group kinetics for the different muscles were linear within error and therefore assessed only as a linear rate over time,  $R_{\text{rep}}^{\text{linear}}$ , in units of mM/h. These rates were comparable for the different muscles, namely  $1.6 \pm 1.8$  mM/h (95% confidence interval (CI): 0.6–2.7 mM/h),  $1.8 \pm 1.4$  mM/h (95% CI: 1.0–2.6 mM/h),  $0.7 \pm 2.2$  mM/h (95% CI: -0.6–2.0 mM/h), and

$1.3 \pm 1.0$  mM/h (95% CI: 0.7–1.9 mM/h) for lateral gastrocnemius (LG), MG, soleus and whole-slice, respectively over the 6 h post exercise (Fig. 2m). On average,  $\Delta[\text{Gly}(0)]_{\text{dep}}^{\text{ex}}$  in LG, MG, soleus, and whole slice in 14 participants was  $45 \pm 14$  mM (95% CI: 37–52 mM),  $37 \pm 14$  mM (95% CI: 28–45 mM),  $35 \pm 17$  mM (95% CI: 25–45 mM), and  $33 \pm 11$  mM (95% CI: 27–39 mM), respectively (Fig. 2l). Over the first 3 h post exercise, the amounts of muscle glycogen repleted ( $\Delta[\text{Gly}(3\text{hr})]_{\text{rep}}$ ) were  $10 \pm 11$  mM (95% CI: 4–16 mM),  $7 \pm 15$  mM (95% CI: -1–16 mM),  $6 \pm 11$  mM (95% CI: 0–12 mM) and  $7 \pm 8$  mM (95% CI: 2–11 mM), respectively.  $\Delta[\text{Gly}(3\text{hr})]_{\text{rep}}$  and  $R_{\text{rep}}^{\text{initial}}$  were positively correlated with  $\Delta[\text{Gly}(0)]_{\text{dep}}^{\text{ex}}$  (Fig. 2n and Supplementary Fig. 7),  $R = 0.79$  and  $R = 0.63$ , respectively. The correlation between 3 h repletion and depletion can be described by the equation:  $\Delta[\text{Gly}(3\text{hr})]_{\text{rep}} = 0.61 \times \Delta[\text{Gly}(0)]_{\text{dep}}^{\text{ex}} - 15$ , suggesting that the initial repletion was a function of glycogen depletion by exercise, and that repletion was positive ( $\Delta[\text{Gly}]_{\text{rep}} > 0$ ) when  $\Delta[\text{Gly}(0)]_{\text{dep}}^{\text{ex}} > 25$  mM. Notice that the intercept is negative, reflecting a few cases where depletion continued before repletion started.



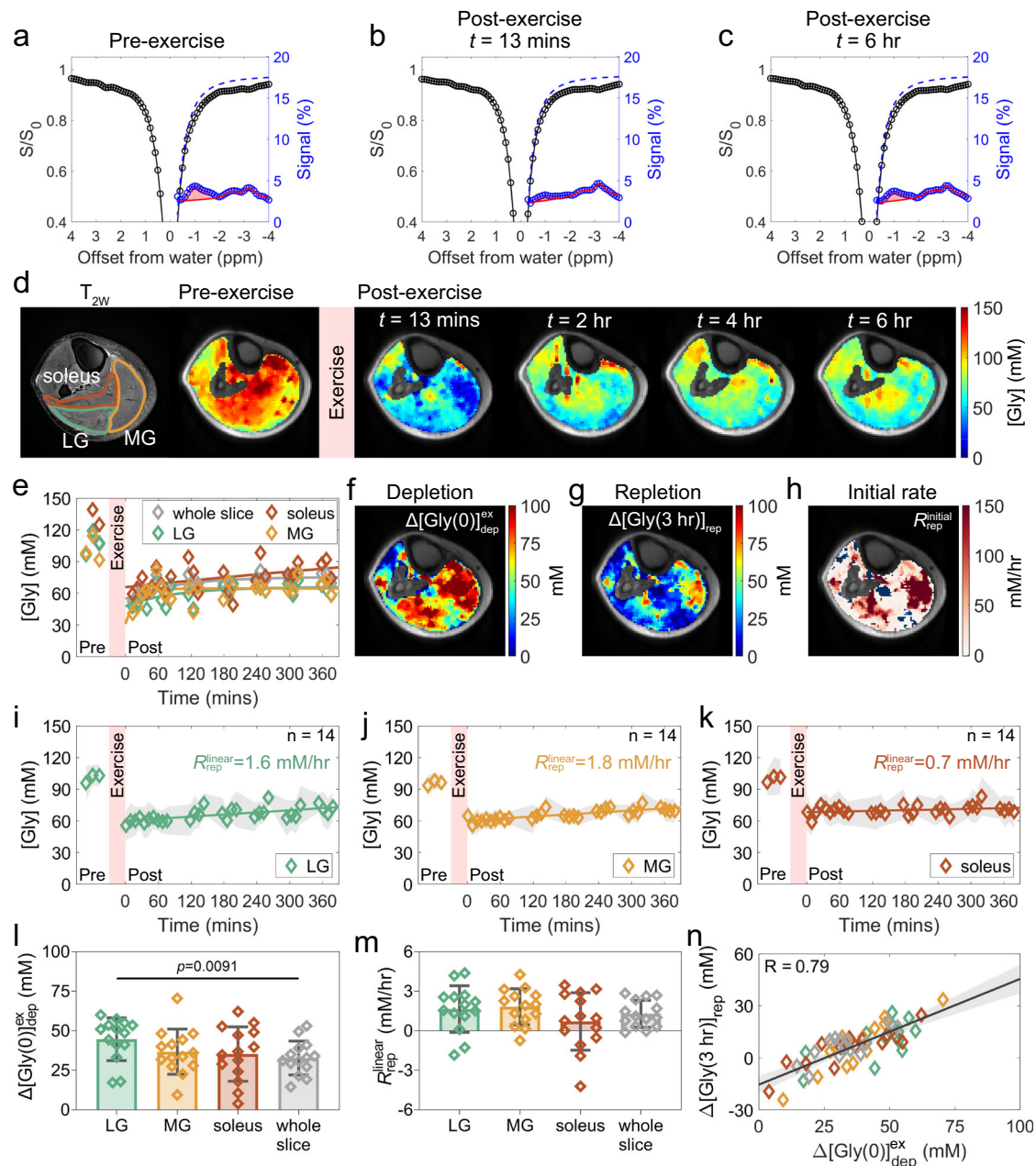


**Fig. 2 | In vivo mapping of glycogen levels in human skeletal muscle before and after 31-min lower intensity plantar flexion exercise.** Whole muscle glycoNOE signals were fitted from the Z-spectra for a representative subject (#1, male) at **a** rest, **b** 13 min post exercise, and **c** 6 h post exercise. **d** Muscle assignment from  $T_{2w}$  MRI and glycogen concentration maps before and after exercise obtained as a function of time. **e** Glycogen levels as a function of time in muscle groups labeled on the  $T_{2w}$  image. **f** Map of amount of glycogen depletion after exercise:  $\Delta[\text{Gly}(0)]_{\text{dep}}^{\text{ex}} = [\text{Gly}]^{\text{base}} - [\text{Gly}(0)]$ . **g** Map of amount of glycogen repletion over the first 3 h:  $\Delta[\text{Gly}(3\text{hr})]_{\text{rep}} = [\text{Gly}(3\text{hr})] - [\text{Gly}(0)]$ . **h** Map of glycogen initial repletion rate  $R_{\text{rep}}^{\text{initial}}$  of the exponential recovery. **i, j, k** Group average ( $n = 14$  subjects per muscle group) of glycogen levels as a function of time for LG, MG, and soleus.

Group analysis ( $n = 14$  subjects per muscle group) for different muscle groups of glycogen I depletion amount  $\Delta[\text{Gly}(0)]_{\text{dep}}^{\text{ex}}$  and **m** linear repletion rate  $R_{\text{rep}}^{\text{linear}}$ . Data are presented as mean  $\pm$  SD. Statistical significance was determined using two-tailed unpaired Wilcoxon rank-sum test.  $p < 0.05$  were considered statistically significant. **n** Correlation and linear regression between glycogen depletion and glycogen repletion over 3 h post exercise ( $n = 14$  subjects). The data points were indicated using the same color coding as in **(m)** for different muscle groups. The gray shadows in **(i–k)** indicate SD, and in **(n)** indicate 95% confidence interval (CI). Slice thickness = 5 mm,  $B_1 = 0.2 \mu\text{T}$ ,  $t_{\text{sat}} = 3$  s,  $\text{TR} = 4$  s. LG lateral gastrocnemius, MG medial gastrocnemius. Source data are provided as a Source Data file.

### Glycogen repletion after higher intensity exercise

We then zoomed in on the initial hours of muscle glycogen recovery post exercise and studied another 14 physically active but untrained male subjects under higher intensity exercise (estimated total mechanical work of 20 to 30 kJ). Figure 3a–d show the glycogen maps for a representative subject that presented high depletion  $\Delta[\text{Gly}(0)]_{\text{dep}}^{\text{ex}}$  (up to 100 mM, Fig. 3c) and high repletion over the first 3 h (Fig. 3d) in a

core region of soleus, indicating a spatial correlation between the two parameters. While the LG and MG presented slow linear repletion, the soleus for this subject showed a high exponential recovery of glycogen, possibly due to high glycogen repletion in the region (Fig. 3e–g). The average repletion curves for 14 participants under higher intensity exercise showed overall linear repletion, with average rates  $R_{\text{rep}}^{\text{linear}}$  ranging from 0.8 mM/h to 3.3 mM/h for different muscle groups

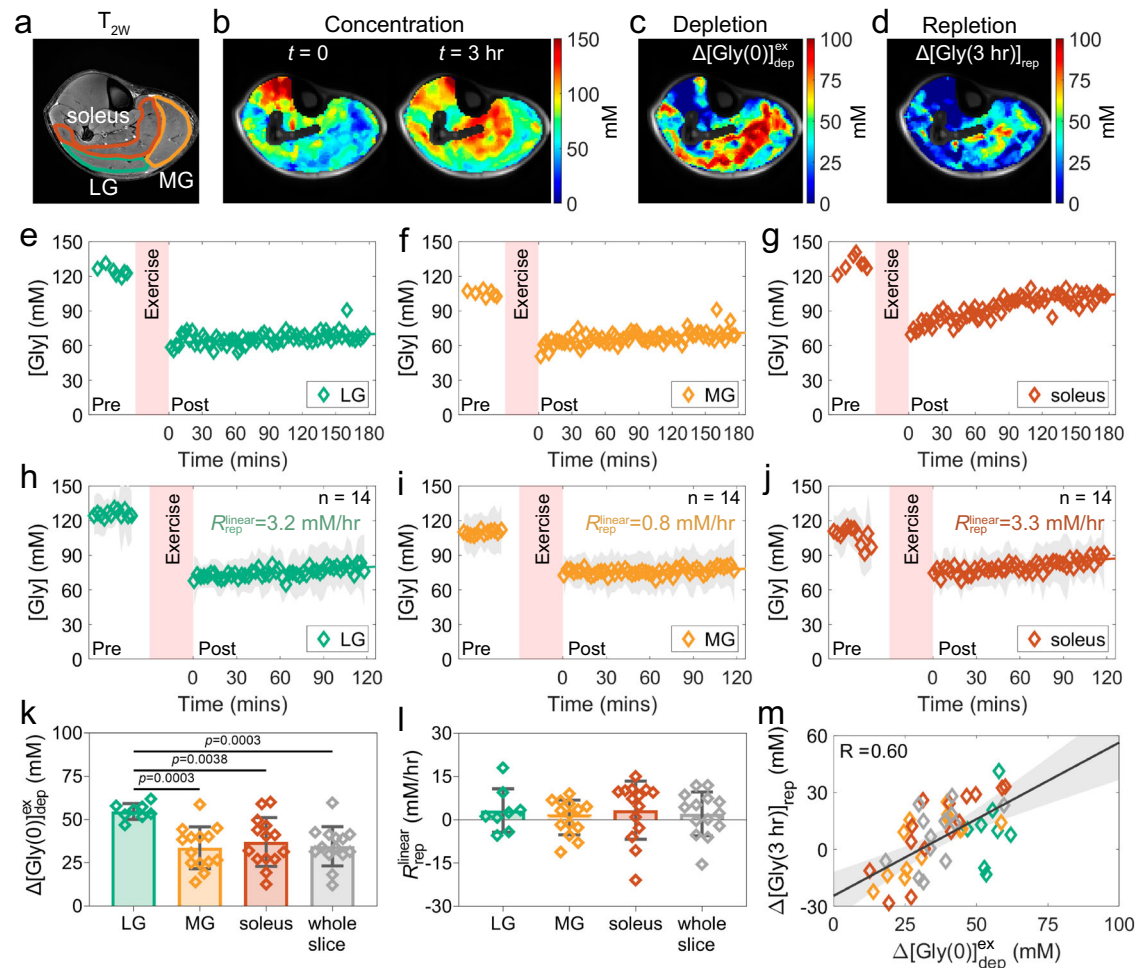


**Fig. 3 | In vivo mapping of glycogen levels in human skeletal muscle before and after 31-min higher intensity plantar flexion exercise.** Muscle a  $T_{2w}$  MRI and maps of b glycogen at  $t = 0, 3$  h post exercise, c glycogen depletion, and d repletion over first 3 h for a representative subject (#15). e–g Glycogen levels as a function of time in muscle groups labeled on the  $T_{2w}$  image. Group average ( $n = 14$  subjects per muscle group) of glycogen levels as a function of time for h LG, i MG, and j soleus. Group analysis ( $n = 14$  subjects per muscle group) for different muscle groups of glycogen k depletion  $\Delta[\text{Gly}(0)]_{\text{dep}}^{\text{ex}}$  and l linear repletion rate  $R_{\text{rep}}^{\text{linear}}$ . Data are

presented as means  $\pm$  SD. Statistical significance was determined using two-tailed unpaired Wilcoxon rank-sum test.  $p < 0.05$  were considered statistically significant. m Correlation and linear regression between glycogen depletion and glycogen repletion over first 3 h post exercise ( $n = 14$  subjects). The data points were indicated using the same color coding as in (l) for different muscle groups. The gray shadows in (h–j) indicate SD, and in (m) indicate 95% CI. Slice thickness = 20 mm,  $B_1 = 0.2 \mu\text{T}$ ,  $t_{\text{sat}} = 1775$  ms,  $\text{TR} = 2$  s. Source data are provided as a Source Data file.

(Fig. 3h–j). On average, LG muscle glycogen was reduced by  $55 \pm 5$  mM (95% CI: 51–59 mM), a level significantly higher than MG ( $34 \pm 12$  mM, 95% CI: 27–41 mM), soleus ( $37 \pm 14$  mM, 95% CI: 29–45 mM), and whole slice ( $35 \pm 11$  mM, 95% CI: 28–41 mM), respectively (Fig. 3k). Their respective linear repletion rates over 3 h post exercise ( $R_{\text{rep}}^{\text{linear}}$  (3hr), Fig. 3l) were not significantly different, and were  $3.2 \pm 7.5$  mM/h (95% CI:  $-3.1$ – $9.5$  mM),  $0.8 \pm 6.0$  mM/h (95% CI:  $-2.7$ – $4.3$  mM),  $3.3 \pm 10.1$  mM/h (95% CI:  $-2.5$ – $9.1$  mM), and  $2.1 \pm 7.6$  mM/h (95% CI:  $-2.3$ – $6.5$  mM). Similar to the lower intensity exercise data (Fig. 2n), a positive correlation between  $\Delta[\text{Gly}(3\text{hr})]_{\text{rep}}$  and  $\Delta[\text{Gly}(0)]_{\text{dep}}^{\text{ex}}$  was seen in higher intensity exercise group (Fig. 3m), and can be described by  $\Delta[\text{Gly}(3\text{hr})]_{\text{rep}} = 0.81 \times \Delta[\text{Gly}]_{\text{dep}}^{\text{ex}} - 24$ .

### Three types of muscle-type-independent glycogen repletion kinetics

While the whole muscle slice presented a slow exponential repletion pattern (Fig. 3), local regions within muscles showed different patterns, stressing the need for spatially resolved study of muscle kinetics. Three types of apparent glycogen repletion kinetics were observed in the local regions: type a, a single exponential repletion that does not reach baseline and displays a wide range of initial recovery rates (up to

about 200 mM/h, Fig. 4e, h); type b, a biphasic process consisting of a rapid repletion followed by a depletion phase (Fig. 4f, i), occurring in high glycogen depletion regions (Fig. 4a, k); type c, glycogen depletion is continued during the initial phase after exercise and followed by an exponential repletion (Fig. 4g, j), occurring in regions with low glycogen depletion at time point immediately after exercise (Fig. 4k). Even within the same muscle (e.g., soleus for the subject), the residual glycogen level post exercise can vary substantially, and variable types (types a and c) of glycogen repletion may occur (Fig. 4a). This significant spatial variation of glycogen utilization and repletion was also seen along the length of soleus and MG muscles when data were collected using a longitudinal field of view (FOV, Fig. 4d and Supplementary Fig. 8). The biphasic glycogen recovery dynamics were also observed along the length of MG and soleus (e.g., type c in MG). Like data collected in the axial view (Fig. 4a), the apparent boundaries between regions of the three types appeared not to align with the anatomical boundaries (Fig. 4d). The glycogen curves for type b and c regions were thus fitted using a biphasic exponential model, giving the rates in phases I and II as well as the transition time point from phase I to phase II ( $t_{\text{trans}}$ ). Figure 4b, c show maps of the glycogen initial repletion rates over the calf slice during phase I and phase II,

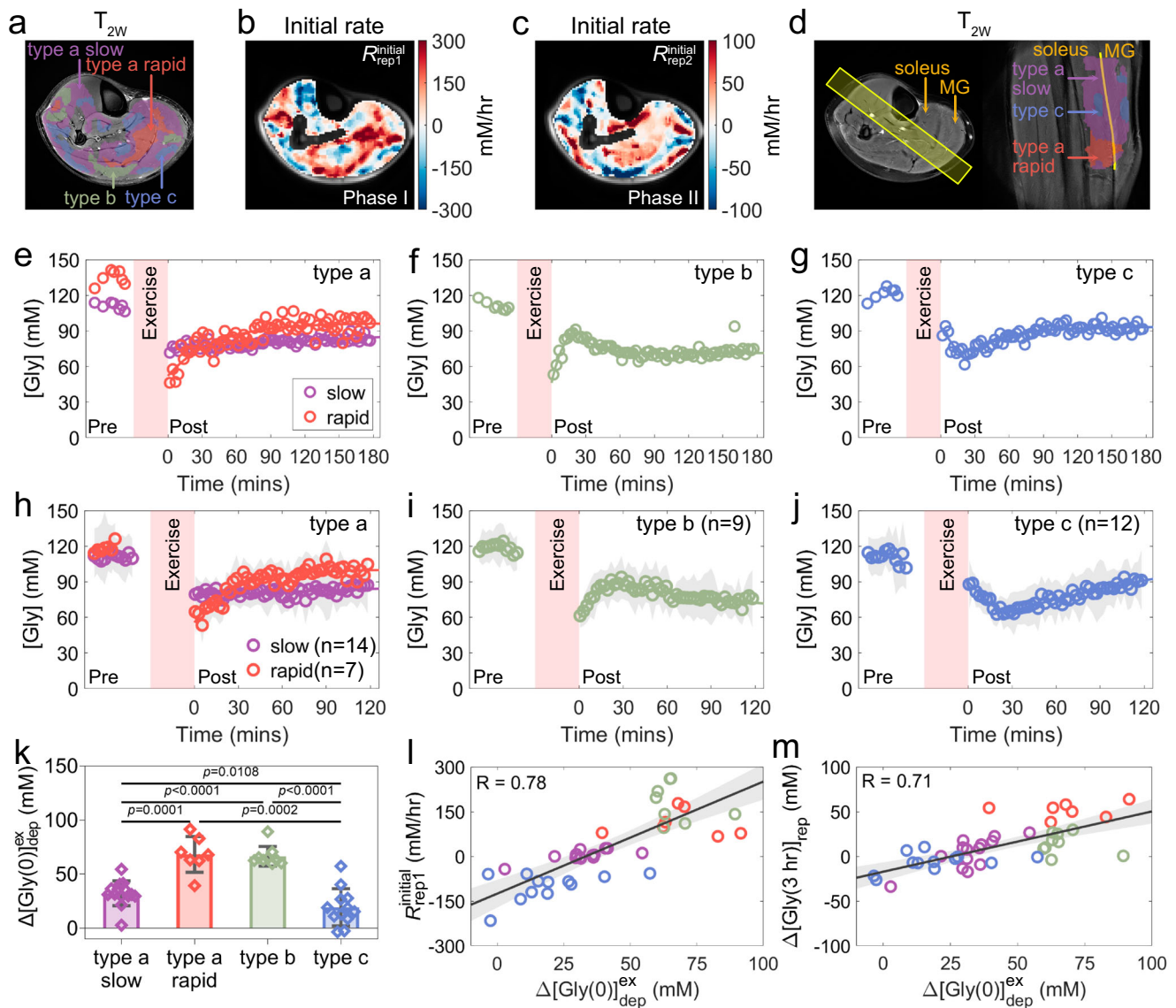


**Fig. 4 | Regional glycogen depletion and repletion patterns in muscle after higher intensity exercise.** **a**  $T_{2W}$  image in the axial view showing regions with the three types of glycogen repletion. The estimated initial rate ( $R_{rep1}^{initial}$  and  $R_{rep2}^{initial}$ ) maps in **b** phase I and **c** phase II, respectively, for the multiphase recoveries (types b and c) in subject #15. **d**  $T_{2W}$  images with overlay showing different types of repletion along the length of MG and soleus for a representative subject (#23). The measured glycogen levels as a function of time in muscle regions with type a (**e**), type b (**f**), and type c (**g**) kinetics, as indicated in (**a**). **h–j** Group average ( $n = 14, 7, 9$ , and  $12$  subjects for type a slow, type a rapid, type b, and type c, respectively) of glycogen levels as a function of time in regions with type a, b, and c kinetics. **k** Group analysis ( $n = 14, 7,$

$9$ , and  $12$  subjects for type a slow, type a rapid, type b, and type c, respectively) of glycogen depletion amount  $\Delta[Gly(0)]_{dep}^{ex}$  for the three types of kinetics. Data are presented as mean  $\pm$  SD. Statistical significance was determined using two-tailed unpaired Wilcoxon rank-sum test.  $p < 0.05$  were considered statistically significant. Correlation and linear regression between glycogen depletion and initial repletion rates of phase I (**l**) and glycogen repletion over 3 h post exercise (**m**) ( $n = 14$  subjects). The data points were indicated using the same color coding as in (**a**) for the respective types of kinetics. The gray shadows indicate SD in (**h–j**) and 95% CI in (**l, m**). Source data are provided as a Source Data file.

respectively, indicating a spatial correlation of glycogen repletion in phase I (e.g., initial rates in Fig. 4l and repletion amount in Supplementary Fig. 8i) with the amount of glycogen depletion. Figure 4k shows the average amount of glycogen depletion at time immediately post exercise for muscle regions with the three types of repletion kinetics in 14 volunteers. The type b region exhibited the highest glycogen depletion ( $\Delta[Gly(0)]_{dep}^{ex} = 67 \pm 9$  mM, 95% CI: 59–74 mM) and initial repletion rate ( $193 \pm 74$  mM/h, 95% CI: 136–249 mM/h), followed by type a (depletion of  $44 \pm 22$  mM, 95% CI: 34–54 mM). Type c region presented lower initial glycogen depletion ( $19 \pm 17$  mM, 95% CI: 8–30 mM), yet high continued initial depletion rates ( $-100 \pm 46$  mM/h, 95% CI:  $-129$  to  $-70$  mM/h). Similar to the muscle group analysis (Fig. 3), the initial repletion rates and the repletion amount over first

3 h post exercise were both positively correlated with glycogen depletion  $\Delta[Gly(0)]_{dep}^{ex}$  when muscles were categorized based on repletion dynamics (Fig. 4l, m).

Table 1 summarizes the respective muscle volume fractions over the imaging slices and fitted parameters for three types of glycogen repletion processes after exercise for 14 volunteers participating in higher intensity exercise (also Supplementary Figs. 8–10 and Supplementary Tables 2 and 3). Around  $78 \pm 12\%$  (in the range of 63–100%) of the muscle regions displayed the type a repletion, followed by  $14 \pm 10\%$  (0–30%) for type c and  $8 \pm 9\%$  (0–28%) for type b. The transition time points post exercise for the biphasic transition ( $t_{trans}$ ) in types b and c were comparable, namely  $26 \pm 6$  min and  $29 \pm 7$  min, respectively. At  $t_{trans}$ , the glycogen concentrations



**Table 1 | Three types of apparent glycogen recovery kinetics in human muscle after higher intensity exercise**

Type*	Volume (%)	$\Delta[\text{Gly}(\text{O})]_{\text{dep}}^{\text{ex}}$ (mM)	Phase I		Transition		Phase II		
			$k_1$ ( $\text{hr}^{-1}$ )	$\Delta[\text{Gly}]_{\text{rep1}}^{\text{ss}}$ (mM)	$t_{\text{trans}}$ (min)	$[\text{Gly}(t_{\text{trans}})]$ (mM)	$k_2$ ( $\text{h}^{-1}$ )	$\Delta[\text{Gly}]_{\text{rep2}}^{\text{ss}}$ (mM)	
a	slow	78 ± 12	32 ± 11	0.7 ± 0.9	3 ± 54	/	/	/	/
	rapid		68 ± 17	2.2 ± 0.8	52 ± 9	/	/	/	/
b	14 ± 10	67 ± 9	3.3 ± 1.9	71 ± 25	26 ± 6	96 ± 12	2.0 ± 1.9	-48 ± 36	
c	8 ± 9	19 ± 17	1.4 ± 1.2	-80 ± 15	29 ± 7	61 ± 11	2.0 ± 1.5	38 ± 23	

\*The type a repletion presented a single phase, was treated as “phase I”, and the transition and phase II sections were left as blank in the table.  $\Delta[\text{Gly}]_{\text{rep1}}^{\text{ss}}$  and  $\Delta[\text{Gly}]_{\text{rep2}}^{\text{ss}}$  are the fitted glycogen repletion amount at steady state for phases I and II, respectively.  $\Delta[\text{Gly}]_{\text{rep1}}^{\text{ss}} = [\text{Gly}]^{\text{ss1}} - [\text{Gly}(\text{O})]$ ;  $\Delta[\text{Gly}]_{\text{rep2}}^{\text{ss}} = [\text{Gly}]^{\text{ss2}} - [\text{Gly}(t_{\text{trans}})]$ , where  $[\text{Gly}]^{\text{ss1}}$  and  $[\text{Gly}]^{\text{ss2}}$  are glycogen concentrations at the (imaginary) steady state for phases I and II, respectively. Values are reported as the mean ± SD ( $n = 14$  subjects) among participants (Supplementary Tables 2 and 3).

$[\text{Gly}(t_{\text{trans}})]$  were about  $96 \pm 12$  mM for type b and  $61 \pm 11$  mM for type c.

## Discussion

Using a glycogen MRI approach developed for humans with a spatial resolution of millimeters and temporal resolution of minutes, the results reveal several new insights into muscle glycogen recovery from exercise. Firstly, muscle glycogen in local regions could undergo continued depletion processes (e.g., the phase I of type c) post exercise. This suggests that glycogenolysis (by glycogen phosphorylase, GPase) is quantitatively important and non-negligible in human muscle post exercise. Secondly, to date there remains uncertainty about the upper limit of glycogen synthesis rates in exercised muscles, as previous  $^{13}\text{C}$  MRS studies<sup>3,20</sup> only measured the averaged kinetics over a large volume. By studying the glycogen kinetics at an improved spatial resolution, the regional maximum rate of glycogen repletion in heavily exercised muscle was revealed to be as high as about 200 mM/h (Fig. 4) during the initial phase of glycogen recovery post exercise, a value much higher than previously reported (around 30 mM/h)<sup>3,20</sup>. Thirdly, a spatial correlation was found between the initial repletion (rate and amount) and the exercise induced glycogen depletion within muscles, indicating a mechanism to reduce the spatial heterogeneity in glycogen distribution during the initial recovery. The substantial temporal and spatial heterogeneity of muscle glycogen kinetics demonstrates the necessity of studying energetics in humans with high resolution.

The mapping of glycogen using ST MRI may be affected by several factors, including the choice of calibration sample, physiological changes, signal background, and errors due to body movement,  $B_1$  and  $B_0$  inhomogeneity. Firstly, glycoNOE signal is known to be influenced by glycogen particle size (Fig. 1c)<sup>41,42</sup>, the choice of a glycogen concentration calibration sample with a similar size distribution as human glycogen is non-trivial. Glycogen samples with a size (26 nm) comparable to human muscle<sup>44,45</sup> were therefore made and used as a concentration calibration reference. During and after exercise, however, glycogen particle size may decrease substantially<sup>13,45–48</sup>, and the degree of the changes is a function of the type of exercise and recovery (Supplementary Table 1). To account for possible particle size changes post exercise, we used the observation that particle size is correlated with glycogen concentration in human muscle (Supplementary Fig. 6) and proposed an algorithm to correct the particle size effects when converting glycoNOE to  $[\text{Gly}]$  (see Methods). Instead of assuming an average particle size for all muscle regions, the proposed approach estimates a particle size for each voxel at each time point. This allows us to correct repletion rates voxel by voxel. The absolute rates of recovery after correction were slightly different from when ignoring particle size changes (Supplementary Fig. 11).

Secondly, the glycoNOE peak may in principle be affected by the direct water saturation (DS) and MTC background in vivo. Increasing  $B_1$  can increase glycoNOE signal in vitro, but it also increases the interference from DS and MTC background, especially at lower magnetic field strength (3–5 T) in vivo (Fig. 1d). Therefore, to obtain a relatively

clean glycogen signal from Z-spectra, an optimal  $B_1$  of 0.2  $\mu\text{T}$  was used for the field of 5T with a fast spin echo (FSE) readout where the train of readout pulses could potentially further contribute to the glycoNOE contrast. In addition,  $T_2$  variations occur during exercise<sup>49,50</sup>, which manifest in the DS signal, possibly affecting glycoNOE detection in certain cases. This can be seen from simulations at 5T (Supplementary Fig. 12) showing that for a reduction in water  $T_2$  to a critically low level (<20 ms), the water DS can broaden substantially and affect glycoNOE visibility in Z-spectra. Yet when  $T_2$  is above the critical level ( $\geq 20$  ms), glycoNOE signals ( $B_1 = 0.2 \mu\text{T}$ ) are stable even when varying  $T_2$ . Consistent with this observation, the substantially different glycoNOEs were similar in 0.5% and 1% agar despite their substantially different  $T_2$  times (223 ms and 115 ms, respectively, Supplementary Table 5). This indicates that  $T_2$  variations (above 30 ms) post exercise are unlikely to affect significantly the glycoNOE measurements for the used  $B_1$ . The muscle  $T_2$  in vivo was above the critical level, and was found to increase from about 30 ms at rest to up to 39 ms and 33 ms at 30 min and 2 h post exercise, respectively (Supplementary Fig. 13). It is worth noting, however, that if muscle  $T_2$  time would decrease below a resting level, for instance, during the administration of glucose or other  $T_2$  contrast agents, the  $T_2$  effects could start to interfere and need to be evaluated and addressed possibly by using an even lower  $B_1$ .

Thirdly, glycoNOEs, unlike glycoCEST effects, have been shown to not be sensitive to pH or temperature within the physiological range<sup>41,42</sup>. The pH insensitivity of glycoNOE is due to the fact that the signal intensity is determined primarily by the NOE transfer rate  $\sigma^{\text{H}}$ , which is not influenced substantially by pH or temperature in the physiological range. In glycoCEST, the signal is determined by the proton exchange rate of hydroxyl protons, which is strongly dependent on pH and temperature. In the two-step glycoNOE process (NOE at slow rate (40–100  $\text{s}^{-1}$ ) followed by proton exchange at high rate (several thousand  $\text{s}^{-1}$ )), the slow step is rate determining. At lower pH (<5), where proton exchange slows down more and rates may become more comparable, a pH dependence can occur<sup>41</sup>.

Fourthly, the glycoNOE signal might be contaminated by other molecular components such as proteins and fatty acids in tissue. For instance, the Z-spectrum for bovine serum albumin (BSA) in vitro displays a peak component near -1 ppm at ultra-high field (15.2T)<sup>51</sup>. We thus evaluated the Z-spectra of mobile proteins and fatty acids in vitro at 37 °C (see Supplementary Results and Discussion). The data (Supplementary Fig. 14) suggest fatty acids show broad major peak components mainly in the range of -2 ppm to -4 ppm of Z-spectra with low  $B_1$  at 5T. BSA shows a broad component from about -0.2 ppm to -4 ppm and beyond. It seems unlikely that only the -1 ppm part of this protein component would change during exercise. We therefore expect protein and fat signals to have minimal contributions to the narrow -1 ppm glycoNOE peak found at 5T in muscle.

Lastly, confounds from several sources, such as motion, muscle swelling,  $B_1$  inhomogeneity, and large blood vessels, may impact the accuracy of the measurement. Motion may cause a mismatch of imaging slices and an alteration of the local field ( $B_0$ ) in voxels. In previous



studies, glycoCEST measurements based on Z-spectrum asymmetry analysis ( $MTR_{\text{asym}}$ ) were found to be highly sensitive to field errors and motions<sup>52,53</sup>. Several successful shim and motion correction approaches have been demonstrated, including water saturation shift referencing (WASSR)<sup>53</sup>, double volumetric navigators (DvNavs)<sup>52,54</sup>, and double-echo gradient-echo as CEST readout (CEST-GRE-2TE)<sup>55</sup>. In this study, the Z-spectra were acquired at low  $B_1$  (0.2  $\mu\text{T}$ ) where the water peak is sharp, and accurate voxel field correction could be performed based on the minimum of the DS water resonance in the voxel-based Z-spectra. To correct muscle swelling or relaxation and motion-related slice mismatch, an image registration step was applied. The  $B_1$  inhomogeneity was accounted for by using a correction algorithm<sup>56</sup> (Supplementary Fig. 4). Using the in vitro data as calibration, the glycogen concentrations in human skeletal muscle measured in this work are about  $99 \pm 13$  mM. Those values are in good agreement with the previously reported human muscle glycogen concentration of 80–110 mM by  $^{13}\text{C}$  MRS<sup>3,4,57,58</sup> and biopsy<sup>4,59</sup>.

Muscle can deplete glycogen storage substantially in relatively short periods of intense exercise (as little as 10 min), during which glycogen is broken down into D-glucose, which then is metabolized to pyruvate/lactate. In this study, we employed a localized exercise protocol that involved repetitive single-leg calf raises in a fully standing position and has been utilized in previous studies<sup>3</sup>. We utilized two different exercise modalities (lower intensity and higher intensity) to investigate the processes of glycogen depletion and repletion. For both groups (Figs. 2 and 3), we assessed the differences between muscles (soleus, MG, and LG) over a 3 to 6 h recovery. The higher intensity group showed a higher baseline level of glycogen ( $[\text{Gly}]^{\text{base}} = 111 \pm 14$  mM) than lower intensity group ( $98 \pm 10$  mM, Figs. 2 and 3). We attribute this to the volunteers in the higher intensity group being more physically active (14 young males, age 22 to 32 years old, representing a moderately to highly active population), which has previously been correlated to higher muscle glycogen storage<sup>59</sup>. The lower intensity group includes 3 females and 11 males representing average population over an age range of 22 to 41 years old. However, the linear repletion rates ( $R_{\text{rep}}^{\text{linear}}$ ) post exercise showed no significant differences between the two groups. In the higher intensity group (Figs. 3 and 4), where a biphasic repletion has been reported<sup>3</sup>, we confirmed the presence of multiple recovery phases during the initial hours after exercise and measured the dynamics with a higher temporal resolution (Fig. 4). While the volunteers were asked to maintain a constant mechanical work output (17 Watts or 31 Watts) during exercise, there were still some variations of working intensity among individuals and different muscles, resulting in a range of residual glycogen levels in exercised calf muscles (Figs. 2–4). Such variability of glycogen utilization within the same muscles and among individuals seems surprising at first sight, yet it agrees with previous reports on heterogeneity in muscle recruitment and energy metabolism under exercise. For instance, studies have established that muscle recruitment is highly heterogeneous<sup>6,8,60,61</sup>, even along the length of muscle, and that the muscle recruitment region does not always match the anatomical boundaries<sup>7,8</sup>.  $^{31}\text{P}$  studies of PCr have suggested that the oxidative capacity of muscle may vary with muscle groups<sup>62</sup> and along the length of the same muscles<sup>63</sup>. It has been known that individuals may have different strategies to recruit muscle for a given exercise<sup>60</sup>. In the current study, the variations in glycogen utilization were seen based on the glycogen depletion map at the high resolution, in line with heterogeneous recruitment patterns and energy metabolism within the same muscles as well as among different muscle groups and individuals.

Glycogen utilization has been reported to depend on muscle fiber type and subcellular location<sup>45</sup>. Type I and type II fibers exhibit different energy metabolic features, due to their differential recruitment preference during exercise and varied expression of enzymes<sup>64,65</sup>. For

instance, in prolonged submaximal exercise, glycogen utilization was more pronounced in type I fibers<sup>65</sup>, suggesting the preferred recruitment of these fibers<sup>66</sup> in aerobic exercise. Interestingly, while soleus had a lower percentage of type II fiber than MG<sup>67,68</sup>, as indicated by the lower pre-exercise levels of carnosine (Supplementary Fig. 15), the glycogen depletion did not differ significantly between the two muscles for the given exercise (Figs. 2 and 3). In addition, no significant spatial correlation ( $p > 0.05$ ) between muscle carnosine level and glycogen repletion (repletion amount and rate) was found (Supplementary Fig. 15) in the higher intensity exercise protocol. At the subcellular level, glycogen is stored in three pools (intermyofibrillar, subsarcolemmal, and intramyofibrillar) at different distances from mitochondria<sup>13</sup>. The utilization and recovery of these three subcellular pools may vary with the ratios of aerobic and anaerobic metabolism, depending on the exercise intensity and duration<sup>46,69</sup>. For instance, it has been suggested that the intermyofibrillar glycogen is utilized preferentially in a 1-min of maximal exercise dominated by anaerobic metabolism, and that intramyofibrillar glycogen is used preferentially in a 15-min of maximal exercise supported mainly by aerobic metabolism<sup>13</sup>. Probing glycogen at a fiber-type level or subcellular level is important<sup>70</sup>, but the spatial resolution of glycoNOE MRI currently precludes the study of such details here.

The current data showed three different types of apparent glycogen recovery in post exercise human muscle, two of which have not been well reported previously (Table 1 and Supplementary Tables 3, 4). While for most regions ( $78 \pm 12\%$ ), a single exponential glycogen repletion process (type a, with a rate constant of  $0.9 \pm 1.1 \text{ h}^{-1}$ ) was typically seen, subjects in the higher intensity exercise group showed biphasic repletion patterns (types b and c) in several local regions. The type a kinetic data are consistent with previous  $^{13}\text{C}$  studies, which reported glycogen repletion rates of  $27 \pm 5$  mM/h in the initial phase and  $2.8 \pm 0.6$  mM/h in the subsequent phase for the studied bulk muscle volumes<sup>3</sup>. However, unlike the previous  $^{13}\text{C}$  studies<sup>3</sup> using a biphasic linear model to describe the glycogen recovery dynamics, here the type a data at high temporal resolution exhibited a mono-exponential recovery pattern. We thus calculated the rate constants ( $k$ ) and initial repletion rates ( $R_{\text{rep}}^{\text{initial}}$ ) with the exponential models to describe the recovery process. Type b regions exhibited a situation where rapid glycogen repletion occurred in phase I ( $R_{\text{rep1}}^{\text{initial}} = 193 \pm 74$  mM/h,  $26 \pm 6$  min), followed by a subsequent depletion phase ( $R_{\text{rep2}}^{\text{initial}} = -50 \pm 33$  mM/h, rate constant of  $2.0 \pm 1.9 \text{ h}^{-1}$ ), which was triggered after glycogen reaching a high level ( $96 \pm 12$  mM). Type c regions showed a continued depletion ( $R_{\text{rep1}}^{\text{initial}} = -100 \pm 46$  mM/h,  $29 \pm 7$  min) immediately after exercise, followed by an exponential repletion stage ( $R_{\text{rep2}}^{\text{initial}} = 50 \pm 33$  mM/h, rate constants of  $2.0 \pm 1.5 \text{ h}^{-1}$ ). The initial repletion rates of phase I ( $R_{\text{rep1}}^{\text{initial}}$ ) were found to be positively correlated with the amount of glycogen depletion (Fig. 4I), in agreement with the previous  $^{13}\text{C}$  results that the initial repletion rates were significantly higher when glycogen was heavily depleted<sup>3,15</sup>. This correlation suggests that muscle tended to reduce the heterogeneity of glycogen storage post exercise by enhancing the initial recovery rates in heavily depleted regions. Consequently, the glycogen maps 2–3 h post exercise often showed a relative homogeneous glycogen distribution over the muscle slice, in contrast to the heterogeneous glycogen depletion immediately after exercise (Figs. 2 and 3). What is particularly interesting here is the observation of regional glycogen depletion (Fig. 4 and Supplementary Figs. 8–10) after higher intensity exercise, suggesting active glycogenolysis in local regions of post exercise muscle. This observation is a strong indirect indication that GPase contribution is quantitatively important during muscle glycogen recovery.

The depletion and repletion of glycogen in muscle is a balanced dynamic (or turnover) of glycogen breakdown and re-synthesis during exercise in vivo<sup>18,71</sup>. Note that lysosomal glycogen exists in muscle cells but only accounts for around 5% of total glycogen<sup>72</sup>, and its

degradation via acid  $\alpha$ -glucosidase during exercise and recovery may be negligible. Therefore, the net rate of glycogen change ( $\Delta[\text{Gly}]/\Delta t$ ) can be described by refs. 18,73:

$$\Delta[\text{Gly}]/\Delta t = R_{\text{syn}} - R_{\text{phos}} \quad (3)$$

$R_{\text{syn}}$  and  $R_{\text{phos}}$  are the rates of glycogen synthesis (by GSase) and glycogen breakdown (rate-limited by GPase), respectively. Previous studies have reported substantial glycogen turnover ( $R_{\text{phos}}/R_{\text{syn}}$ ) in human liver<sup>74</sup> and exercising muscle<sup>48,73</sup>, showing GSase and GPase are active simultaneously. It is clear that active glycogen turnover also occurs post exercise and Eq. 3 also applies to the glycogen repletion dynamics at recovery. The appearance of regional glycogen recovery (Fig. 4) may be understood from the aspect of the post exercise regulation of both GSase and GPase. The rapid glycogen repletion in phase I of types a and b (Table 1) shows that the maximum GSase activity ( $R_{\text{syn}}$ ) can be achieved with a rate of as high as about 200 mM/h in human muscle. This rapid repletion phase is likely a result of the strong activation of GSase as well as the suppression of GPase ( $R_{\text{syn}} > R_{\text{phos}}$ ), which has been observed in rat<sup>25</sup> and human muscles<sup>75,76</sup>. Interestingly, the type c data suggest a rapid glycogen depletion in phase I. This indicates that highly active GPase could be maintained in certain regions after higher intensity exercise for about half an hour. The transition from phase I to phase II (types b and c) indicates a dynamic change in GPase and/or GSase activities during the initial recovery.

The exact regulating mechanism for the biphasic glycogen recovery post exercise remains poorly understood and multiple factors that regulate GSase or GPase may play a role. Considering that the initial repletion rates were positively correlated with glycogen depletion (Fig. 4i), exercise induced factors may be important for the regulation of GSase and GPase during the initial phase of recovery. These may include the enhanced glucose uptake, several-fold increase<sup>77</sup> of glucose 6-phosphate (G6P, an activator of GSase<sup>21</sup> and inhibitor of GPase<sup>78</sup>), the change of glycogen concentration<sup>77,79</sup> and structures<sup>70</sup>, protein kinases, and phosphatases<sup>22,23</sup>. The glycogen re-synthesis ( $R_{\text{syn}}$ ) in muscle relies mainly on the continual supply of blood glucose via a chain of reactions, including glucose transport (by primarily glucose transporter type 4, GLUT4) into cells, phosphorylation to G6P (by hexokinase) and incorporation of UDP-glucose into glycogen by GSase<sup>21</sup>. It has been proposed that the glucose uptake (glucose transporter and/or hexokinase) step is the rate-controlling step of glycogen synthesis by providing a “feed-forward” mechanism to activate GSase via G6P<sup>21</sup>. However, the current data support that both GSase and GPase contribution should be considered during initial hours of muscle glycogen recovery post exercise. The GPase activities in local regions after exercise may play a role in several processes. Firstly, the breakdown of glycogen/glucose produces energy and lactate which can be further oxidized by mitochondria in the same or neighboring cells. The produced energy may support different cellular events, including the re-synthesis of PCr and glycogen. Secondly, the produced lactate may be transported to neighboring muscle regions for glycogen re-synthesis. While the production of glucose from lactate is historically considered to occur mainly in the liver, many studies have shown that the conversion of lactate to glucose/glycogen also exists in skeletal muscle in vivo, and that it might contribute substantially to glycogen synthesis post exercise<sup>80,81</sup>, thus the re-distribution of the overall carbohydrate storage in muscle after exercise. Thirdly, parts of produced lactate may be transported to other organs such as the liver and brain, and used as a substrate for metabolisms.

Caution should be taken when interpreting the glycogen depletion process, as glycogen concentration was derived from glycoNOE under the assumption of a correlation between glycogen concentration and particle size in human muscle. This assumption is based on the observation that both average particle size and concentration in muscle decrease under exercise and increase gradually during

recovery. We thus developed an empirical equation describing the dependence of glycogen concentration on particle size in human tissues based on the glycogen structural model<sup>82</sup> and literature data (Supplementary Methods). Under this assumption, the rapid depletion in type c data (Fig. 4g, j) may be interpreted as a simultaneous decrease in both glycogen concentration and particle size. However, it might be possible that the rapid glycoNOE decrease could be explained by a decrease in particle size alone with minimal concentration changes. For instance, a decrease in glycogen size from 25 nm to 14 nm alone (assuming a constant concentration) may lead to a 50% decrease in glycoNOE signals. In other words, the possibility of a re-distribution of large particles into smaller ones in muscle after exercise cannot be excluded. One study shows that overexpression of glycogenin increases numerical density but not concentration<sup>83</sup>. Another study shows that lowering energy intake is associated with smaller particles in muscle<sup>43</sup>. These studies might suggest that the numeric density of glycogen particles might be prioritized above large particles. Further studies to understand the correlation between glycogen concentration and average particle size in human muscle are needed to provide further insights into this issue.

It is worth noting that the current study was conducted on subjects who fasted for 12 to 18 h (overnight fasting followed by a further 3–6 h of fasting during recovery) and that the observed glycogen recovery kinetics could be affected by factors such as hormonal changes and substrates availability under this fasting condition. Firstly, a decreased release of insulin and increased glucagon and epinephrine under fasting<sup>84</sup> may favor glycogen breakdown and limit glycogen synthesis in muscle. It has been suggested that glucose uptake may be the rate-limiting step for glycogen synthesis<sup>21</sup> and is stimulated by insulin and impaired by glucagon<sup>85,86</sup>. Elevated epinephrine under fasting may enhance glycogen breakdown in muscle, although not necessarily at rest<sup>87</sup>. Interestingly, it has been shown that the initial phase of glycogen repletion is insulin-independent and the following phase insulin-dependent<sup>3</sup>, indicating that exercise induced factors may play a major role in the initial rate of the recovery. Secondly, the availability of glucose and lactate may play a role in glycogen metabolic rates. The respective rates of glucose uptake by GLUT4 and glycogen synthesis increase with blood glucose concentration and are higher when exogenous carbohydrates are available. Lactate may be an additional source for glycogen re-synthesis within the muscle<sup>80</sup>. An enhanced lactate clearance in the liver during fasting might facilitate its clearance in muscle and slow down the glycogen synthesis from lactate<sup>84</sup>. In summary, lower or no carbohydrate intake is associated with slower glycogen concentration recovery and smaller glycogen particle sizes<sup>43</sup>, which could be understood from aspects of impaired glycogen synthesis and stimulated glycogen breakdown due to hormonal regulations and the availability of substrates including glucose and lactate/pyruvate.

We estimate that the glycoNOE approach is at least ten thousand times more sensitive than the traditional nature abundance <sup>13</sup>C MRS in probing the total glycogen pool in human. Only 1.1% (natural abundance) of glycogen C1 (single position) is detectable in <sup>13</sup>C MRS, while 100% of four aliphatic protons (H3, H5, H2 + H4–1) are detected with the enhancement of two orders of magnitude relative to proton MRS<sup>42</sup>. Detecting protons also gives a 32 times sensitivity gain over a <sup>13</sup>C detection<sup>88</sup>. This thus allows relatively fast imaging (currently less than 1 min per scan) of glycogen with a high in-plane spatial resolution (1.6 mm × 1.6 mm × 20 mm) using glycoNOE MRI. In principle, further increasing the time resolution of glycogen kinetics measurements without compromising spatial resolution is feasible via using ultrafast Z-spectrum acquisition schemes<sup>89,90</sup> or simply optimizing the Z-spectral sampling ranges. Previously, glycogen levels in both liver<sup>91,92</sup> and resting muscle<sup>52,53,93</sup> in vivo were assessed using glycoCEST effects of the hydroxyl protons that resonate around +1 ppm in Z-spectrum. However, due to the intermediate to fast chemical exchange rates of

hydroxyl protons *in vivo*, glycoCEST signals are partially coalesced with the water resonance in Z-spectrum, posing a significant challenge to extract the signals accurately, especially at lower fields. In addition, some of these studies use so-called asymmetry analysis with respect to the water frequency at 0 ppm, thus subtracting the glycoNOE from the glycoCEST effect, complicating any interpretation. In future studies, it is worth exploring the simultaneous application of the glycoNOE and glycoCEST in exercising muscle and liver, which is not trivial as the optimal signal change magnitude for these two mechanisms occurs at different  $B_1$  levels. The spatial tracking of glycogen utilization in exercising muscle could provide further insights into muscle energetics and fatigue. Mapping glycogen storage and use dynamics in the liver during events such as fasting and substrate intake would help understand related hepatic metabolisms. In previous studies, glycoCEST experiments on exercising muscle<sup>94</sup> and on liver<sup>95,96</sup> have been shown technically feasible. For instance, the glycoCEST approach has been applied in the human liver with breath-hold<sup>95</sup> and free-breathing<sup>96</sup> protocols. Motion-robust Z-spectra acquisition schemes that integrate techniques such as rapid acquisition, denoising, motion and local field correction approaches<sup>52,54</sup> are desirable for these applications.

In conclusion, we established an approach to measure regional glycogen metabolism in human muscle using MRI. While muscle-type based analysis showed a slow recovery of glycogen levels under fasting conditions after both low and high intensity exercises, regional analysis showed a spatially heterogeneous and temporally biphasic glycogen re-synthesis in post-exercise human skeletal muscle. In some regions, a decrease of glycogen signals during muscle recovery from exercise was observed, suggesting that glycogen phosphorylase may be active and quantitatively important in post-exercise muscles.

## Methods

### Glycogen preparation

To evaluate the effect of glycogen particle size on glycoNOE measurement in muscle, glycogen samples with varied average sizes from about 12 to 28 nm were first made *in vitro* from commercial glycogen (from rabbit liver, type III, G8876, chemical abstract service registry no. 9005-79-2, Sigma, St. Louis) that are ~80 nm in size. Briefly, glycogen solutions were prepared in phosphate-buffered saline (PBS), adjusted to pH 3.0, and incubated for hydrolysis at 80 °C for 1 to about 30 days. The size distributions of glycogen samples were monitored using dynamic light scattering (DLS, Zetasizer Nano ZS, Malvern Instruments). Once degraded glycogen reached a targeted size (e.g., 26 nm), the glycogen solutions were adjusted back to pH 7.3, and centrifuged at 4951 ×g with a 30 kDa cut-off (Millipore Sigma) filter to remove low molecular glucose chains, and subsequently filtered with a 0.1 μm pore-size membrane to remove high molecular precipitates. Then the glycogen in solution was precipitated with 1.5 volumes of ethanol, centrifuged (4951 ×g, 30 min) down, and finally lyophilized for further uses.

### ST MRI

All MRI experiments were conducted using a Jupiter 5T human scanner (United Imaging Healthcare, Shanghai, China) with a 24-channel transmit/receive knee coil. In each ST MRI experiment, multiple Z-spectra were acquired as a function of  $B_1$  (0.1 to 0.5 μT). In each repetition time (TR) of 2 s or 4 s, a continuous wave (CW) pulse was applied, followed by a single-shot FSE readout. For experiments with a TR of 2 s, the durations ( $t_{\text{sat}}$ ) of the CW pulse were set:  $t_{\text{sat}} = \text{TR} - \text{ACQ}$ , where ACQ was the FSE acquisition time, was 225 ms; For experiments with a TR of 4 s,  $t_{\text{sat}}$  was fixed as 3 s. Image resolution was set as 96 × 96, with a 160 mm × 160 mm field of view (FOV) for human. Unless otherwise specified, the saturation frequencies were stepped over a range from -4 to +4 ppm or -3 to +0.6 ppm with step size of 0.1 or 0.2 ppm. The non-saturated image ( $S_0$ ) was collected with saturation

pulse power ( $B_1$ ) set to 0 for normalization.  $B_1$  maps were acquired over the selected slices with a DREAM sequence after Z-spectral scans<sup>97</sup>.

### MRI experiments on glycogen *in vitro*

Three batches of glycogen samples were made and evaluated. (i) Various concentrations of glycogen (20, 40, 60, 80, 100, 200, 300, and 400 mM) solutions with the same particle size of 26 nm were prepared separately with PBS and adjusted to pH 7.3 to calibrate the signal to concentration relationship. (ii) To better represent the solid-like background in tissue *in vivo*, a second batch of samples was prepared with 1% agar in PBS, adjusted to pH 7.3, heated to 90 °C for 2 h, and then cooled. (iii) A group of glycogen samples with the same concentration of 100 mM but varied particle sizes (ranging from 12 nm to 28 nm) were also prepared in PBS. The temperature of samples was maintained at 37 °C during MRI scans with a water bath and a circulation system. The slice thickness was 12 mm for phantoms, frequency ranges from -4 ppm to +4 ppm with a step of 0.1 ppm.

### MRI experiments on human calf at rest

Human studies were approved by the Institutional Review Board of Shenzhen Institute of Advanced Technology and were performed on healthy subjects after informed written consent was obtained. The above ST MRI experiments were performed on the human calf muscle of 16 healthy subjects (50–82 kg in weight, BMI of 18–28 kg/m<sup>2</sup>, 22–41 years old, 13 males and 3 females, with no family history of diabetes) at rest. Participants' sex was determined based on self-report. Sex was not considered in the study design and sex analysis was not carried out due to the limited number of female volunteers responding to the recruitment. The Z-spectral acquisition ranges from -4 ppm to +4 ppm with a step of 0.1 ppm, slice thickness of 5 mm, TR of 4 s, and acquisition time of 5 min 28 s.

### Exercise protocols

A plantar flexion exercise protocol<sup>3</sup> was performed on healthy subjects who avoided intense exercise during the week before experiments. After overnight fasting, each subject's body weight was measured and used to determine the exercise intensity. During the experiments, the subjects were required not to eat but were allowed to drink water. Subjects exercised for 31 min by alternating a 1 min single-leg standing calf raises exercise in a fully standing position with 1 min of rest. The subjects were asked to maintain an average number of raises per min during exercise, which was calculated by: average raises per min = total mechanical work/16 min/(force × distance) = (1 kJ/min)/(force × distance), where total work was targeted to a certain intensity, force = body mass × acceleration of gravity, distance is the average distance that the heel moved. The exact number of raises was counted and used to estimate the real total mechanical work. Two targeted workloads were set in the following protocols.

Protocol A (lower intensity exercise): a total mechanical work of 16 kJ during the 31 min of exercise was set for 14 healthy subjects (53–83 kg in weight, BMI of 18–28 kg/m<sup>2</sup>, 22–41 years old, 11 males and 3 females, with no family history of diabetes) who were from general population with no specific physical requirements. Prior to exercise, three groups of baseline Z-spectra (one group included Z-spectral data under  $B_1 = 0.2, 0.3, 0.1 \mu\text{T}$ , frequency ranges from -4 ppm to +4 ppm, with a step of 0.2 ppm, slice thickness of 5 mm, TR of 4 s and acquisition time of 2 min 48 s) were acquired. Immediately after the plantar flexion exercise, the volunteer was positioned back to the scanner within 3 min, and repetitive Z-spectra were collected during the first 1- to 1.5-h post exercise and at 2, 3, 4, 5, and 6 h post exercise. Pads were placed around the calf to minimize movement during the scanning. Volunteers were asked to rest outside the scanner during intervals of the scans.



Protocol B (higher intensity exercise): a total mechanical work of 30 kJ was set for 14 physically active but untrained male subjects (68–83 kg in weight, BMI of 21–28 kg/m<sup>2</sup>, 22–33 years old, with no family history of diabetes). (i) ST experiments were used to monitor the glycogen change before and after exercise for 8 subjects within a transverse slice of 20 mm thickness and with a temporal resolution of 120 s (three Z-spectra per time point under B<sub>1</sub> = 0.2, 0.3, 0.1 μT, frequency ranges from -3 to +0.6 ppm, with a step of 0.2 ppm, TR = 2 s, 40 s per Z-spectral acquisition). See details in Supplementary Methods on increasing the temporal resolution of glycogen mapping. (ii) To study the glycogen dynamics along the length of muscles, the same exercise protocol was applied to 6 subjects, a FOV parallel to the bone was set to cover partial volumes of soleus and MG. The frequency list in ST experiments was -8, -7, -6, -5, -4, -3, -2.8, ..., 0.4, 0.6 ppm, TR = 2 s, 50 s per Z-spectral acquisition. T<sub>2</sub> maps were acquired over the calf muscle for 6 volunteers at rest and at 25, 50, 75, and 100 min post exercise, using a multi-echo spin-echo sequence with a TR of 1000 ms and the echo times (TE) of 24, 47, 71, 95, 119, 142, 166, and 190 ms. The slice thickness in protocol B was set four times (20 mm) that (5 mm) of protocol A, to capture the initial phase of glycogen recovery with an improved signal noise ratio. To assess the stability of the dynamic measurements, a group of 1.5- to 2-h repetitive scans were performed on the non-exercised leg of each volunteer on a different day.

### Data analysis

To account for body motion during the MRI scan after exercise, in vivo CEST images at each saturation frequency as well as S<sub>0</sub> images were first registered to a reference image (S<sub>0</sub> image) of the last CEST acquisition post exercise for each subject. Next, all of the Z-spectra were analyzed in a voxel-by-voxel manner. The exercise Z-spectral data were interpolated to a step of 0.1 ppm. B<sub>0</sub> shifts of Z-spectra were corrected with the WASSR method<sup>53</sup>. After normalization with S<sub>0</sub>, a Z-spectrum based B<sub>1</sub>-correction method with smoothing spine interpolation was performed to compensate for B<sub>1</sub> inhomogeneity<sup>56</sup>. The Z-spectra were then referenced to the Z-spectral intensity at -4 ppm of an example subject to eliminate mismatches in the background signal of Z-spectra between subjects<sup>37</sup>. The signal of interest (glycoNOE) is mixed with a broad background consisting of contributions from DS, rNOEs, and MTC, but becomes better visible in the residual spectrum when background (DS + MTC) is estimated and removed from the Z-spectrum. A two-step multi-pool Lorentzian fitting approach was developed to quantify glycoNOE signal from the Z-spectrum, as shown in Supplementary Fig. 3. Firstly, a multi-pool Lorentzian fitting was performed to estimate the background (DS + MTC) signal in the Z-spectrum. MTC was estimated from a reference full Z-spectrum (frequency ranging from -10 ppm to +10 ppm) and fixed in the fitting. Then the residual spectrum was further fitted with a multi-pool Lorentzian fitting to extract the glycoNOE signal. More details of data processing were in the Supplementary Methods.

We introduced an algorithm to account for the glycogen particle size changes in the concentration calculation after exercise. The measured glycogen concentration in human muscle was shown to depend on the average particle size (*d*, see the derivation in Supplementary Methods), described empirically by:

$$[\text{Gly}(d)] = A(1.2^d - 1) \quad (4)$$

where A = 0.9005 mM. Based on Eqs. 1, 2, we have,

$$\text{glycoNOE}(d) = [\text{Gly}(d)] \times \text{slope}(26\text{nm}) \times \alpha(d) \quad (5)$$

Thus,

$$\text{glycoNOE}(d) = A(1.2^d - 1) \times \text{slope}(26\text{nm}) \times (0.004 \times d^2 + 0.0287 \times d - 0.0176) \quad (6)$$

Here, slope(26 nm) and A are known constants. To convert the glycoNOE<sub>*i*</sub> signal to [Gly]<sub>*i*</sub> in the *i*-th voxel, the particle size *d<sub>i</sub>* was first estimated from Eq. 6, after which α(*d<sub>i</sub>*) was obtained from Eq. 2 and [Gly]<sub>*i*</sub> was determined in Eq. 4.

For the muscle regions identified on T<sub>2w</sub> MRI, the glycogen dynamic curve ([Gly(*t*))] was assumed to be a single exponential recovery (type a):

$$[\text{Gly}(t)] = [\text{Gly}(0)] + \Delta[\text{Gly}]_{\text{rep}}^{\text{SS}} (1 - e^{-k_{\text{rep}}t}) \quad (7)$$

*k<sub>rep</sub>* is the repletion rate constant. *t* is the time after completion of exercise. Δ[Gly]<sub>rep</sub><sup>SS</sup> = [Gly]<sup>SS</sup> - [Gly(0)], where [Gly]<sup>SS</sup> and [Gly(0)] are the concentrations at steady state (*t* → ∞) and starting point (*t* = 0), respectively. The initial rate of the exponential recovery at *t* = 0 (*R<sub>rep</sub>*<sup>initial</sup>) was calculated by: *R<sub>rep</sub>*<sup>initial</sup> = d[Gly(*t*)]/dt(*t* = 0) = Δ[Gly]<sub>rep</sub><sup>SS</sup> × *k<sub>rep</sub>* × e<sup>-*k<sub>rep</sub>**t*</sup>(*t* = 0) = Δ[Gly]<sub>rep</sub><sup>SS</sup> × *k<sub>rep</sub>*. When analyzing muscle group repletion, the curves for each group based on T<sub>2w</sub> assignment were also assessed with a linear model: [Gly(*t*)] = [Gly(0)] + *R<sub>rep</sub>*<sup>linear</sup> × *t*. *R<sub>rep</sub>*<sup>linear</sup> is the linear rate, in units of mM/h.

For certain heavily exercised regions, the time dependence of glycoNOE signals post exercise showed a biphasic exponential pattern (types b and c), which were assessed with the following piecewise function:

$$[\text{Gly}(t)] = \begin{cases} [\text{Gly}(0)] + \Delta[\text{Gly}]_{\text{rep1}}^{\text{SS}} (1 - e^{-k_1t}), & 0 < t < t_{\text{trans}} \\ [\text{Gly}(t_{\text{trans}})] + \Delta[\text{Gly}]_{\text{rep2}}^{\text{SS}} \{1 - e^{-k_2(t-t_{\text{trans}})}\}, & t > t_{\text{trans}} \end{cases} \quad (8)$$

*k<sub>1</sub>* and *k<sub>2</sub>* are the repletion (or depletion) rate constants in phases I and II, respectively. Δ[Gly]<sub>rep1</sub><sup>SS</sup> = [Gly]<sup>SS1</sup> - [Gly(0)] and Δ[Gly]<sub>rep2</sub><sup>SS</sup> = [Gly]<sup>SS2</sup> - [Gly(*t<sub>trans</sub>*)], where [Gly]<sup>SS1</sup> and [Gly]<sup>SS2</sup> are the fitted glycogen concentrations at steady state (*t* → ∞) for the two phases, respectively, [Gly(*t<sub>trans</sub>*)] is the glycogen level at the transition point *t<sub>trans</sub>*. The respective initial rates of phase I (at *t* = 0) and phase II (at *t* = *t<sub>trans</sub>*) recovery were: *R<sub>rep1</sub>*<sup>initial</sup> = Δ[Gly]<sub>rep1</sub><sup>SS</sup> × *k<sub>1</sub>* and *R<sub>rep2</sub>*<sup>initial</sup> = Δ[Gly]<sub>rep2</sub><sup>SS</sup> × *k<sub>2</sub>*.

The uncertainties of the above fitted repletion parameters were estimated using 2000 Monte Carlo simulations of the kinetic data with a similar random noise level estimated based on the volume of interest (VOI). Data processing was performed using custom-written scripts on MATLAB (Mathworks, Natick, MA, USA). Statistical tests were performed with Prism9 (GraphPad Software). Groups were considered significantly different when two-tailed unpaired Wilcoxon rank-sum test analysis showed *p*-value of 0.05 or less between groups.

### Reporting summary

Further information on research design is available in the Nature Portfolio Reporting Summary linked to this article.

### Data availability

All data supporting the findings of this study are available in the article and the Supplementary Information and from the corresponding author upon request. The raw MRI data generated in this study are available on Open Science Framework at <https://osf.io/8AF6W/98>. Requests for additional data should be submitted to: Y.Z. via yang.zhou@siat.ac.cn. Please expect a 2-week response time. Source data are provided with this paper.

### Code availability

The analysis code used in this study is available on Open Science Framework at <https://osf.io/8AF6W/98>.

### References

- Jue, T. et al. Direct observation of glycogen synthesis in human muscle with <sup>13</sup>C NMR. *Proc. Natl. Acad. Sci. USA* **86**, 4489–4491 (1989).



2. Jensen, J., Rustad, P., Kolnes, A. & Lai, Y.-C. The role of skeletal muscle glycogen breakdown for regulation of insulin sensitivity by exercise. *Front. Physiol.* **2**, 112 (2011).
3. Price, T. B. et al. Human muscle glycogen resynthesis after exercise: insulin-dependent and -independent phases. *J. Appl. Physiol.* **76**, 104–111 (1994).
4. Taylor, R., Price, T. B., Rothman, D. L., Shulman, R. G. & Shulman, G. I. Validation of  $^{13}\text{C}$  NMR measurement of human skeletal muscle glycogen by direct biochemical assay of needle biopsy samples. *Magn. Reson. Med.* **27**, 13–20 (1992).
5. Hargreaves, M. & Spriet, L. L. Skeletal muscle energy metabolism during exercise. *Nat. Metab.* **2**, 817–828 (2020).
6. Masood, T. et al. Differential contributions of ankle plantarflexors during submaximal isometric muscle action: a PET and EMG study. *J. Electromyogr. Kinesiol.* **24**, 367–374 (2014).
7. Bojsen-Møller, J., Schwartz, S., Kalliokoski, K. K., Finni, T. & Magnusson, S. P. Intermuscular force transmission between human plantarflexor muscles in vivo. *J. Appl. Physiol.* **109**, 1608–1618 (2010).
8. Staudenmann, D., Kingma, I., Daffertshofer, A., Stegeman, D. F. & van Dieën, J. H. Heterogeneity of muscle activation in relation to force direction: a multi-channel surface electromyography study on the triceps surae muscle. *J. Electromyogr. Kinesiol.* **19**, 882–895 (2009).
9. Vieira, T. M. M., Loram, I. D., Muceli, S., Merletti, R. & Farina, D. Postural activation of the human medial gastrocnemius muscle: are the muscle units spatially localised? *J. Appl. Physiol.* **589**, 431–443 (2011).
10. Vigh-Larsen, J. F., Ørtenblad, N., Spriet, L. L., Overgaard, K. & Mohr, M. Muscle glycogen metabolism and high-intensity exercise performance: a narrative review. *Sports Med.* **51**, 1855–1874 (2021).
11. Laaksonen, M. S. et al. Regional differences in blood flow, glucose uptake and fatty acid uptake within quadriceps femoris muscle during dynamic knee-extension exercise. *Eur. J. Appl. Physiol.* **113**, 1775–1782 (2013).
12. Jensen, R. et al. Heterogeneity in subcellular muscle glycogen utilisation during exercise impacts endurance capacity in men. *J. Physiol.* **598**, 4271–4292 (2020).
13. Schytz, C. T., Ørtenblad, N., Gejl, K. D. & Nielsen, J. Differential utilisation of subcellular skeletal muscle glycogen pools: a comparative analysis between 1 and 15 min of maximal exercise. *J. Appl. Physiol.* **602**, 1681–1702 (2024).
14. Burke, L. M., van Loon, L. J. C. & Hawley, J. A. Postexercise muscle glycogen resynthesis in humans. *J. Appl. Physiol.* **122**, 1055–1067 (2016).
15. Price, T. B., Rothman, D. L. & Shulman, R. G. NMR of glycogen in exercise. *Proc. Nutr. Soc.* **58**, 851–859 (1999).
16. Rothman, D. L., Magnusson, I., Katz, L. D., Shulman, R. G. & Shulman, G. I. Quantitation of hepatic glycogenolysis and gluconeogenesis in fasting humans with  $^{13}\text{C}$  NMR. *Science* **254**, 573–576 (1991).
17. Price, T. B., Rothman, D. L., Avison, M. J., Buonamico, P. & Shulman, R. G.  $^{13}\text{C}$ -NMR measurements of muscle glycogen during low-intensity exercise. *J. Appl. Physiol.* **70**, 1836–1844 (1991).
18. Price, T. B. et al. Turnover of human muscle glycogen with low-intensity exercise. *Med. Sci. Sports Exerc.* **26**, 983–991 (1994).
19. Delmas-Beauvieux, M. C. et al.  $^{13}\text{C}$  nuclear magnetic resonance study of glycogen resynthesis in muscle after glycogen-depleting exercise in healthy men receiving an infusion of lipid emulsion. *Diabetes* **48**, 327–333 (1999).
20. Price, T. B. et al. NMR studies of muscle glycogen synthesis in insulin-resistant offspring of parents with non-insulin-dependent diabetes mellitus immediately after glycogen-depleting exercise. *Proc. Natl. Acad. Sci. USA* **93**, 5329–5334 (1996).
21. Shulman, R., Bloch, G. & Rothman, D. In vivo regulation of muscle glycogen synthase and the control of glycogen synthesis. *Proc. Natl. Acad. Sci. USA* **92**, 8535–8542 (1995).
22. Roach, P. J., Depaoli-Roach, A. A., Hurley, T. D. & Tagliabracci, V. S. Glycogen and its metabolism: some new developments and old themes. *Biochem. J.* **441**, 763–787 (2012).
23. Katz, A. A century of exercise physiology: key concepts in regulation of glycogen metabolism in skeletal muscle. *Eur. J. Appl. Physiol.* **122**, 1751–1772 (2022).
24. Sandström, M. E. et al. Insulin-independent glycogen super-compensation in isolated mouse skeletal muscle: role of phosphorylase inactivation. *Pflugers Arch. Eur. J. Physiol.* **448**, 533–538 (2004).
25. BrÄU, L. et al. Regulation of glycogen synthase and phosphorylase during recovery from high-intensity exercise in the rat. *Biochem. J.* **322**, 303–308 (1997).
26. Blackwood, S. J., Hanya, E. & Katz, A. Effect of postexercise temperature elevation on postexercise glycogen metabolism of isolated mouse soleus muscle. *J. Appl. Physiol.* **126**, 1103–1109 (2019).
27. Katz, A. The role of glycogen phosphorylase in glycogen biogenesis in skeletal muscle after exercise. *Sports Med. Health Sci.* **5**, 29–33 (2023).
28. Blackwood, S. J., Hanya, E. & Katz, A. Heating after intense repeated contractions inhibits glycogen accumulation in mouse EDL muscle: role of phosphorylase in postexercise glycogen metabolism. *Am. J. Physiol. Cell Physiol.* **315**, C706–C713 (2018).
29. Forsén, S. & Hoffman, R. A. Study of moderately rapid chemical exchange reactions by means of nuclear magnetic double resonance. *J. Chem. Phys.* **39**, 2892–2901 (1963).
30. van Zijl, P. C. M. & Yadav, N. N. Chemical exchange saturation transfer (CEST): what is in a name and what isn't? *Magn. Reson. Med.* **65**, 927–948 (2011).
31. Ward, K. M., Aletras, A. H. & Balaban, R. S. A new class of contrast agents for MRI based on proton chemical exchange dependent saturation transfer (CEST). *J. Magn. Reson.* **143**, 79–87 (2000).
32. Zhou, Y., Bie, C., van Zijl, P. C. M. & Yadav, N. N. The relayed nuclear Overhauser effect in magnetization transfer and chemical exchange saturation transfer MRI. *NMR Biomed.* **36**, e4778 (2022).
33. Henkelman, R. M., Stanisz, G. J. & Graham, S. J. Magnetization transfer in MRI: a review. *NMR Biomed.* **14**, 57–64 (2001).
34. Balaban, R. S. & Ceckler, T. L. Magnetization transfer contrast in magnetic resonance imaging. *Magn. Reson. Q.* **8**, 116–137 (1992).
35. Pike, G. B. Pulsed magnetization transfer contrast in gradient echo imaging: a two-pool analytic description of signal response. *Magn. Reson. Med.* **36**, 95–103 (1996).
36. van Zijl, P. C. M., Lam, W. W., Xu, J., Knutsson, L. & Stanisz, G. J. Magnetization transfer contrast and chemical exchange saturation transfer MRI. Features and analysis of the field-dependent saturation spectrum. *NeuroImage* **168**, 222–241 (2018).
37. Chen, L. et al. Investigation of the contribution of total creatine to the CEST Z-spectrum of brain using a knockout mouse model. *NMR Biomed.* **30**, e3834 (2017).
38. Kogan, F. et al. Method for high-resolution imaging of creatine in vivo using chemical exchange saturation transfer. *Magn. Reson. Med.* **71**, 164–172 (2014).
39. Chen, L., Barker, P. B., Weiss, R. G., van Zijl, P. C. M. & Xu, J. Creatine and phosphocreatine mapping of mouse skeletal muscle by a polynomial and Lorentzian line-shape fitting CEST method. *Magn. Reson. Med.* **81**, 69–78 (2019).
40. Chen, L. et al. In vivo imaging of phosphocreatine with artificial neural networks. *Nat. Commun.* **11**, 1072 (2020).
41. Zhou, Y., van Zijl, P. C. M., Xu, J. & Yadav, N. N. Mechanism and quantitative assessment of saturation transfer for water-based detection of the aliphatic protons in carbohydrate polymers. *Magn. Reson. Med.* **85**, 1643–1654 (2021).
42. Zhou, Y. et al. Magnetic resonance imaging of glycogen using its magnetic coupling with water. *Proc. Natl. Acad. Sci. USA* **117**, 3144–3149 (2020).

43. Maehlum, S. & Hermansen, L. Muscle glycogen concentration during recovery after prolonged severe exercise in fasting subjects. *Scand. J. Clin. Lab. Invest.* **38**, 557–560 (1978).
44. Ryu, J.-H. et al. Comparative structural analyses of purified glycogen particles from rat liver, human skeletal muscle and commercial preparations. *Int. J. Biol. Macromol.* **45**, 478–482 (2009).
45. Hokken, R. et al. Subcellular localization- and fibre type-dependent utilization of muscle glycogen during heavy resistance exercise in elite power and Olympic weightlifters. *Acta Physiol.* **231**, e13561 (2021).
46. Marchand, I. et al. Quantitative assessment of human muscle glycogen granules size and number in subcellular locations during recovery from prolonged exercise. *J. Physiol.* **580**, 617–628 (2007).
47. Gejl, K. D. et al. Local depletion of glycogen with supramaximal exercise in human skeletal muscle fibres. *J. Appl. Physiol.* **595**, 2809–2821 (2017).
48. Marchand, I. et al. Quantification of subcellular glycogen in resting human muscle: granule size, number, and location. *J. Appl. Physiol.* **93**, 1598–1607 (2002).
49. Ploutz-Snyder, L. L., Nyren, S., Cooper, T. G., Potchen, E. J. & Meyer, R. A. Different effects of exercise and edema on  $T_2$  relaxation in skeletal muscle. *Magn. Reson. Med.* **37**, 676–682 (1997).
50. Varghese, J. et al. Rapid assessment of quantitative  $T_1$ ,  $T_2$  and  $T_2^*$  in lower extremity muscles in response to maximal treadmill exercise. *NMR Biomed.* **28**, 998–1008 (2015).
51. Jin, T. & Kim, S.-G. Role of chemical exchange on the relayed nuclear Overhauser enhancement signal in saturation transfer MRI. *Magn. Reson. Med.* **87**, 365–376 (2022).
52. Simegn, G. L., Van der Kouwe, A. J. W., Robertson, F. C., Meintjes, E. M. & Alhamud, A. Real-time simultaneous shim and motion measurement and correction in glycoCEST MRI using double volumetric navigators (DvNavs). *Magn. Reson. Med.* **81**, 2600–2613 (2019).
53. Kim, M., Gillen, J., Landman, B. A., Zhou, J. & Van Zijl, P. C. Water saturation shift referencing (WASSR) for chemical exchange saturation transfer (CEST) experiments. *Magn. Reson. Med.* **61**, 1441–1450 (2009).
54. Simegn, G. L., Alhamud, A., van der Kouwe, A. J. W., Meintjes, E. & Robertson, F. Repeatability and reproducibility of prospective motion- and shim corrected 2D glycoCEST MRI. *Quant. Imaging Med. Surg.* **9**, 1674–1685 (2019).
55. Poblador Rodriguez, E. et al. A comparison of static and dynamic  $\Delta B_0$  mapping methods for correction of CEST MRI in the presence of temporal  $B_0$  field variations. *Magn. Reson. Med.* **82**, 633–646 (2019).
56. Windschuh, J. et al. Correction of  $B_1$ -inhomogeneities for relaxation-compensated CEST imaging at 7 T. *NMR Biomed.* **28**, 529–537 (2015).
57. Goforth, H. W. et al. Effects of depletion exercise and light training on muscle glycogen supercompensation in men. *Am. J. Physiol. Endocrinol. Metab.* **285**, E1304–E1311 (2003).
58. Heinicke, K. et al. Reproducibility and absolute quantification of muscle glycogen in patients with glycogen storage disease by  $^{13}\text{C}$  NMR spectroscopy at 7 Tesla. *PLoS ONE* **9**, e108706 (2014).
59. Areta, J. L. & Hopkins, W. G. Skeletal muscle glycogen content at rest and during endurance exercise in humans: a meta-analysis. *Sports Med.* **48**, 2091–2102 (2018).
60. Finni, T., Hodgson, J. A., Lai, A. M., Edgerton, V. R. & Sinha, S. Muscle synergism during isometric plantarflexion in achilles tendon rupture patients and in normal subjects revealed by velocity-encoded cine phase-contrast MRI. *Clin. Biomech.* **21**, 67–74 (2006).
61. Kinugasa, R., Kawakami, Y. & Fukunaga, T. Muscle activation and its distribution within human triceps surae muscles. *J. Appl. Physiol.* **99**, 1149–1156 (2005).
62. Larsen, R. G., Callahan, D. M., Foulis, S. A. & Kent-Braun, J. A. In vivo oxidative capacity varies with muscle and training status in young adults. *J. Appl. Physiol.* **107**, 873–879 (2009).
63. Boss, A. et al. Oxidative capacity varies along the length of healthy human tibialis anterior. *J. Appl. Physiol.* **596**, 1467–1483 (2018).
64. Lowry, C. V. et al. Enzyme patterns in single human muscle fibers. *J. Biol. Chem.* **253**, 8269–8277 (1978).
65. Ball-Burnett, M., Green, H. J. & Houston, M. E. Energy metabolism in human slow and fast twitch fibres during prolonged cycle exercise. *J. Physiol.* **437**, 257–267 (1991).
66. Gollnick, P. D., Piehl, K. & Saltin, B. Selective glycogen depletion pattern in human muscle fibres after exercise of varying intensity and at varying pedalling rates. *J. Physiol.* **241**, 45–57 (1974).
67. Baguet, A. et al. A new method for non-invasive estimation of human muscle fiber type composition. *PLoS ONE* **6**, e21956 (2011).
68. Lievens, E., Klass, M., Bex, T. & Derave, W. Muscle fiber typology substantially influences time to recover from high-intensity exercise. *J. Appl. Physiol.* **128**, 648–659 (2020).
69. Nielsen, J., Holmberg, H. C., Schrøder, H. D., Saltin, B. & Ortenblad, N. Human skeletal muscle glycogen utilization in exhaustive exercise: role of subcellular localization and fibre type. *J. Physiol.* **589**, 2871–2885 (2011).
70. Shearer, J. & Graham, T. E. Novel aspects of skeletal muscle glycogen and its regulation during rest and exercise. *Exerc. Sport Sci. Rev.* **32**, 120–126 (2004).
71. Constable, S. H., Young, J. C., Higuchi, M. & Holloszy, J. O. Glycogen resynthesis in leg muscles of rats during exercise. *Am. J. Physiol.* **247**, R880–R883 (1984).
72. Calder, P. C. & Geddes, R. Rat skeletal muscle lysosomes contain glycogen. *Int. J. Biochem.* **21**, 561–567 (1989).
73. Laurent, D. et al. Mechanism of muscle glycogen autoregulation in humans. *Am. J. Physiol. Endocrinol. Metab.* **278**, E663–E668 (2000).
74. Magnusson, I. et al. Liver glycogen turnover in fed and fasted humans. *Am. J. Physiol. Endocrinol. Metab.* **266**, E796–E803 (1994).
75. Richter, E. A. Is GLUT4 translocation the answer to exercise-stimulated muscle glucose uptake? *Am. J. Physiol. Endocrinol. Metab.* **320**, E240–E243 (2020).
76. Montell, E., Arias, A. & Gómez-Foix, A. M. Glycogen depletion rather than glucose 6-P increments controls early glycogen recovery in human cultured muscle. *Am. J. Physiol. Regul. Integr. Comp. Physiol.* **276**, R1489–R1495 (1999).
77. Price, T. B., Laurent, D., Petersen, K. F., Rothman, D. L. & Shulman, G. I. Glycogen loading alters muscle glycogen resynthesis after exercise. *Eur. J. Appl. Physiol.* **88**, 698–704 (2000).
78. Bloch, G. et al. In vivo regulation of rat muscle glycogen resynthesis after intense exercise. *Am. J. Physiol. Endocrinol. Metab.* **266**, E85–E91 (1994).
79. Jensen, J. & Lai, Y.-C. Regulation of muscle glycogen synthase phosphorylation and kinetic properties by insulin, exercise, adrenaline and role in insulin resistance. *Arch. Physiol. Biochem.* **115**, 13–21 (2009).
80. Jin, E. S., Sherry, A. D. & Malloy, C. R. Evidence for reverse flux through pyruvate kinase in skeletal muscle. *Am. J. Physiol. Endocrinol. Metab.* **296**, E748–E757 (2009).
81. Donovan, C. M. & Pagliassotti, M. J. Quantitative assessment of pathways for lactate disposal in skeletal muscle fiber types. *Med. Sci. Sports Exerc.* **32**, 772–777 (2000).
82. Goldsmith, E., Sprang, S. & Fletterick, R. Structure of maltoheptaose by difference Fourier methods and a model for glycogen. *J. Mol. Biol.* **156**, 411–427 (1982).
83. Skurat, A. V., Lim, S.-S. & Roach, P. J. Glycogen biogenesis in rat 1 fibroblasts expressing rabbit muscle glycogenin. *Europ. J. Biochem.* **245**, 147–155 (1997).
84. Karimi, R., Clevon, A., Elbarbry, F. & Hoang, H. The impact of fasting on major metabolic pathways of macronutrients and pharmacokinetics steps of drugs. *Eur. J. Drug Metab. Pharmacokin.* **46**, 25–39 (2021).

85. Chen, S.-S. et al. Glucagon chronically impairs hepatic and muscle glucose disposal. *Am. J. Physiol. Endocrinol. Metab.* **292**, E928–E935 (2007).
86. Richter, E. A. & Hargreaves, M. Exercise, GLUT4, and skeletal muscle glucose uptake. *Physiol. Rev.* **93**, 993–1017 (2013).
87. Laurent, D., Petersen, K. F., Russell, R. R., Cline, G. W. & Shulman, G. I. Effect of epinephrine on muscle glycogenolysis and insulin-stimulated muscle glycogen synthesis in humans. *Am. J. Physiol. Endocrinol. Metab.* **274**, E130–E138 (1998).
88. Levitt, M. H. *Spin Dynamics: Basics of Nuclear Magnetic Resonance* (Wiley, 2001).
89. Xu, X., Lee, J.-S. & Jerschow, A. Ultrafast scanning of exchangeable sites by NMR spectroscopy. *Angew. Chem. Int. Ed.* **52**, 8281–8284 (2013).
90. Bie, C., van Zijl, P. C. M., Mao, D. & Yadav, N. N. Ultrafast Z-spectroscopic imaging in vivo at 3T using through-slice spectral encoding (TS-UFZ). *Magn. Reson. Med.* **89**, 1429–1440 (2023).
91. van Zijl, P. C., Jones, C. K., Ren, J., Malloy, C. R. & Sherry, A. D. MRI detection of glycogen in vivo by using chemical exchange saturation transfer imaging (glycoCEST). *Proc. Natl. Acad. Sci. USA* **104**, 4359–4364 (2007).
92. Deng, M. et al. Chemical exchange saturation transfer (CEST) MR technique for liver imaging at 3.0 Tesla: an evaluation of different offset number and an after-meal and over-night-fast comparison. *Mol. Imaging Biol.* **18**, 274–282 (2016).
93. Simegn, G. L., Alhamud, A., Robertson, F. & van der Kouwe, A. J. W. Chemical exchange saturation transfer MRI optimal continuous wave RF irradiation parameters for glycogen (glycoCEST) detection. *Appl. Magn. Reson.* **51**, 621–640 (2020).
94. Rerich, E., Zaiss, M., Korzowski, A., Ladd, M. E. & Bachert, P. Relaxation-compensated CEST-MRI at 7 T for mapping of creatine content and pH—preliminary application in human muscle tissue in vivo. *NMR Biomed.* **28**, 1402–1412 (2015).
95. Chen, S.-Z. et al. Chemical exchange saturation transfer (CEST) MR technique for in-vivo liver imaging at 3.0 tesla. *Eur. Radiol.* **26**, 1792–1800 (2016).
96. Han, P. et al. Free-breathing 3D CEST MRI of human liver at 3.0 T. *Magn. Reson. Med.* **89**, 738–745 (2023).
97. Nehrke, K. & Börner, P. DREAM—a novel approach for robust, ultrafast, multislice  $B_1$  mapping. *Magn. Reson. Med.* **68**, 1517–1526 (2012).
98. Bie, C. et al. In vivo imaging of glycogen in human muscle. *Open Science Framework*. <https://osf.io/8AF6W/> (2023).
- (2022J05013). P.v.Z and N.Y. are supported by NIH grants P41 EB031771 and R01 NS127280.

### Author contributions

Y.Z. and C.B. conceived the study and designed the experiments; C.B., Y.M., X.X., C.Z., and Y.Z. performed the experiments; C.B., P.v.Z., L.C., J.L.A., C.Z. and Y.Z. analyzed the data; Y.Z., C.B., P.v.Z., and N.Y. wrote the manuscript; H.Z., D.L., C.Z., J.L.A., and L.C. edited the manuscript; all authors discussed the results and approved the final version of the manuscript.

### Competing interests

P.v.Z., Y.Z., and N.Y. have filed a patent application (PCT/US2021/060214) for the glycoNOE approach. The other authors declare that they have no competing interests.

### Additional information

**Supplementary information** The online version contains supplementary material available at <https://doi.org/10.1038/s41467-024-55132-x>.

**Correspondence** and requests for materials should be addressed to Yang Zhou.

**Peer review information** *Nature Communications* thanks Anders Aagaard Hansen, Joachim Nielsen, Jeanine Prompers, and the other, anonymous, reviewer(s) for their contribution to the peer review of this work. A peer review file is available.

**Reprints and permissions information** is available at <http://www.nature.com/reprints>

**Publisher's note** Springer Nature remains neutral with regard to jurisdictional claims in published maps and institutional affiliations.

**Open Access** This article is licensed under a Creative Commons Attribution-NonCommercial-NoDerivatives 4.0 International License, which permits any non-commercial use, sharing, distribution and reproduction in any medium or format, as long as you give appropriate credit to the original author(s) and the source, provide a link to the Creative Commons licence, and indicate if you modified the licensed material. You do not have permission under this licence to share adapted material derived from this article or parts of it. The images or other third party material in this article are included in the article's Creative Commons licence, unless indicated otherwise in a credit line to the material. If material is not included in the article's Creative Commons licence and your intended use is not permitted by statutory regulation or exceeds the permitted use, you will need to obtain permission directly from the copyright holder. To view a copy of this licence, visit <http://creativecommons.org/licenses/by-nc-nd/4.0/>.

© The Author(s) 2024

### Acknowledgements

This work was supported by the National Natural Science Foundation of China (82171904, 82302151), Shenzhen Science and Technology Program (JCYJ20220818101213029), Postdoctoral Fellowship Program of CPSF (GZC20241846), Key Laboratory for Magnetic Resonance and Multimodality Imaging of Guangdong Province (2023B1212060052), National Key Research and Development Program of China (2022YFA1004203), Scientific Program of Guangdong Province (2022B151520068), Fujian Province Science and Technology Project